Separation and Purification Technology 316 (2023) 123811

Contents lists available at ScienceDirect

Separation and Purification Technology

journal homepage: www.elsevier.com/locate/seppur

# Electrochemical reduction of $CO_2$ into formate/formic acid: A review of cell design and operation

Dina Ewis [a], Muhammad Arsalan [a], Mazen Khaled [b], Deepak Pant [c], Muneer M. Ba-Abbad [a], Abdulkarem Amhamed [d], Muftah H. El-Naas [a,*]

[a] Gas Processing Center, College of Engineering, Qatar University, P.O.Box 2713, Doha, Qatar
[b] Department of Chemistry and Earth, Qatar University, Doha, Qatar
[c] Separation & Conversion Technology, Flemish Institute for Technological Research (VITO), Boeretang 200, 2400 Mol, Belgium
[d] Qatar Environment & Energy Research Institute, Hamad Bin Khalifa University, Education City, Doha, Qatar

ARTICLE INFO

*Keywords:*
Electrochemical reduction of $CO_2$
Formate
Formic acid
Cell design
$CO_2$ conversion

ABSTRACT

The release of carbon dioxide ($CO_2$) into the atmosphere is threatening the environment and ecosystems, resulting in major challenges to sustainable development for modern industry. In this context, $CO_2$ electrochemical reduction ($CO_2$ ECR) is one of the most promising technologies to mitigate the effects of high $CO_2$ content in the atmosphere. Electrochemical technology can convert $CO_2$ into value-added chemicals including methanol, ethanol and formate. In this review, different mechanisms of $CO_2$ electrochemical reduction into formate/formic acid are reviewed, highlighting the different cell designs . Also, the effect of cell design and operating parameters on the electrochemical reduction process are discussed. The review aims to highlight recent developments in the $CO_2$ electrochemical cell design for formate production and provide guidelines for future advancements. Challenges of large-scale production and research gaps are also provided.

## 1. Introduction

The anthropogenic emissions of $CO_2$ due to the unprecedented utilization of fossil fuels have resulted in detrimental environmental consequences, threatening living communities. It has been reported that the level of $CO_2$ reached 421 ppm in 2022 and it could reach up to 790 ppm by 2100 with the current industrial emissions [1]. Therefore, it is important to switch energy and chemical production from fossil fuels to renewable energy resources through energy conversion and storage technologies with net zero $CO_2$ emissions popularly known as the Power-to-X approach [2]. The $CO_2$ electrochemical reduction ($CO_2$ ECR) is a promising technology that provides various chemical productions including alcohols, hydrocarbons, and formate. These chemicals are used as long-term energy storage materials that can effectively replace the products derived from fossil fuels. Therefore, this technology can effectively close the anthropogenic carbon cycle, reduce the $CO_2$ level in the atmosphere, and reach $CO_2$ neutral economy. Formic acid is an intermediate value feedstock that is used in textile industries, pharmaceutical industry and agriculture. In fact, it is an essential chemical that is used as a preservative, antibacterial agent, and in hydrogen storage [3]. Formate, an equilibrium product of formic acid, can be further processed into hydrocarbons through the Fischer-Tropsch process [4]. It is worth noting that in $CO_2$ ECR, formate or formic acid can be selectively produced by manipulating the electrolyte pH as will be discussed in Section 3.1.2 [5,6].

Besides $CO_2$ ECR technology, other technologies including photochemical, photoelectrochemical, biochemical, and thermochemical for $CO_2$ conversion are also available. Yet, $CO_2$ ECR has great potential owing to its operation under ambient conditions (temperature and pressure), practical operation, and possible integration with renewable energy resources for efficient power supply as will be discussed later. However, $CO_2$ ECR systems still suffer from issues related to catalyst stability [7], low selectivity, competitive reactions, and byproduct impurities [8,9].

Despite the fact that most studies are dedicated to developing effective electrocatalysts, there is a good number of research articles that examined the influence of operation conditions, cell configuration, and design parameters on the production of formate/formic acid. Based on the current literature, most review articles on $CO_2$ ECR to formate/formic acid are limited to the synthesis of electrocatalysts. For instance,

---

* Corresponding author.
*E-mail addresses:* mkhaled@qu.edu.qa (M. Khaled), muftah@qu.edu.qa (M.H. El-Naas).

https://doi.org/10.1016/j.seppur.2023.123811
Received 25 January 2023; Received in revised form 5 April 2023; Accepted 5 April 2023

Zhang et al.[10] reviewed the $CO_2$ ECR mechanism and the catalysts used for formate production discussing their properties and performance. While Al-Tamreh et al. [11] provided an overview of the $CO_2$ ECR into formate process, focusing on the catalysts used and providing guidelines for efficient catalysts design, however, this paper provided a general overview of the types of electrolysis cells without discussing the effect of design factors, operation parameters and cell configuration on formate production. Liang et al.[12] reviewed the $CO_2$ ECR electrolysis cells design without focusing on the cells examined specifically for formate/formic acid production and the influence of the operating parameters. Duarah et al.[13] offered a comprehensive review on the most common catalysts used for $CO_2$ ECR to formic acid. The authors outlined the effect of temperature and pressure on the conversion process and highlighted the techno-economic feasibility of formic acid production via $CO_2$ ECR. Masel et al. [14] reviewed the current advances in formate/formic acid production focusing on catalysts for industrial application. In this context, the current review summarizes the electrolysis cell designs for formate/formic acid production, focusing on their features, advantages, and disadvantages. In addition, the review discusses the effect of operational (e.g. feed pattern and temperature) and design (e.g. electrode size, cell configuration) parameters on the formate/formic acid production. Finally, large-scale production and challenges related to cell design and operation are presented as well.

## 2. Principle of $CO_2$ electrochemical reduction into formate/formic acid

Electrochemical reduction (ECR) of $CO_2$ is the process by which $CO_2$ is reduced to chemical products by electrical energy in the presence of an electrocatalyst, which interacts with the $CO_2$ and the solution components resulting in an electron exchange process [15]. In a conventional electrolytic cell, the system consists of cathodic and anodic compartments separated by a membrane to prevent mixing of the electroreduction products. In both compartments, electrodes are placed in an electrolyte medium, which is an ion-conducting phase, and connected to an external power supply to initiate the reduction process. When a voltage or current is applied, a strong interaction occurs between the ions in the electrolyte solution and the electrode resulting in the formation of five regions: electrode surface, inner Helmholtz plane (IHP), outer Helmholtz plane (OHP), diffuse layer and bulk solution. The IHP layer consists of adsorbed reactants, intermediates, reaction products, solvent molecules, and solvated electrolyte ions. The adsorbed ions in the IHP are attracted to the electrode through physical and chemical adsorption [16]. The OHP layer consists of solvated non-specifically adsorbed ions that are oppositely charged to the electrode. These ions may interact with the electrode through electrostatic forces. The diffuse layer is comprised of non-specifically adsorbed ions, which extend from the OHP layer to the bulk solution. The Helmholtz layer (IHP and OHP) and the diffuse layer form an electrical double layer (EDL) in which its total charge density equals to the charge of the electrode surface, but with opposite sign. The EDL capacitance depends on the finite size of the ions, ion concentration, type of the ions, the electrode area, and material type. However, there is no general rule that can directly define the influence of these factors on the EDL capacity. Yet, as described in recent literature, surface charge plays a role in enhancement of $CO_2$ RR selectivity by creating a new intermediate, where the stabilization involving strong chemical interactions with the catalyst is suggested due to surface-charging effects [17-20]. It is worth mentioning that the same principles are applied to the EDL capacities of aqueous and nonaqueous solutions, but the capacities are generally lower in aqueous solutions [21]. The reduction of $CO_2$ occurs on the IHP; thereby, it is influenced by the above-mentioned factors besides catalyst selectivity towards $CO_2$, reaction activity and $CO_2$ concentration gradient. The value of the capacity, the structure, and the thickness of EDL play an important role in the electroreduction process in which they can enhance or hinder the reduction process by influencing the faradaic reactions [10,22-24]. Fig. 1 illustrates the formed EDL during the $CO_2$ electroreduction process.

Theoretically, formic acid is produced at an electrochemical potential of −0.250 V vs. RHE at pH 7. However, more negative overpotential is required due to complex reaction mechanisms and sluggish kinetics. The large overpotential is a result of the barrier associated with the initial electron transfer to form $CO_2$ radical intermediate that is poorly stabilized by the electrode surface [25-27]. Unfortunately, the high overpotential occurs at the potential range where hydrogen evolution reaction (HER) can compete with $CO_2$ conversion, which is the main challenge in $CO_2$ ECR. Consequently, developing catalysts with high activity and selectivity that are capable of accelerating the reaction

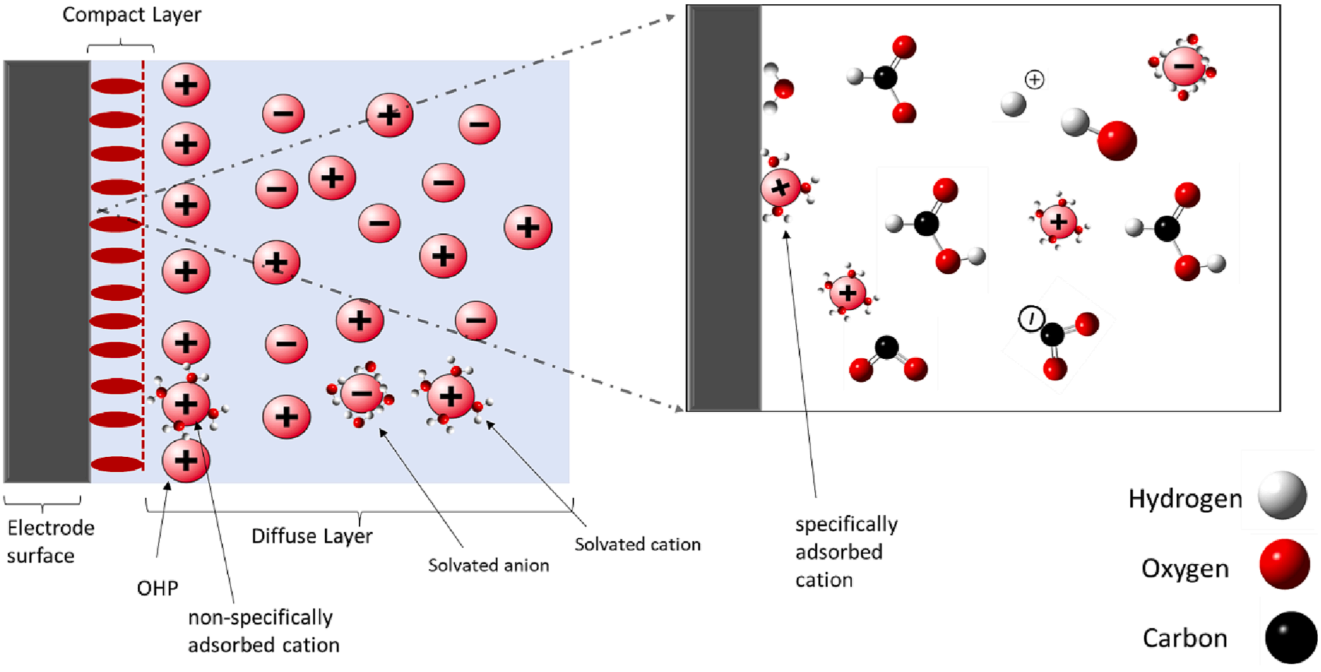

**Fig. 1.** Electrode double layer structure at the cathode.

kinetics and efficiency by lowering the reduction potential of $CO_2$ is the main focus of most research activities [28,29]. The mechanism of $CO_2$ ECR to formate/formic acid is not yet fully understood. It has been reported, however, that the mechanism involves three main steps: (1) the adsorption of the reactant on the surface of the working electrode (2) electron and proton transfer (3) desorption of the products from the working electrode. The mechanism is revealed through computational, electrokinetics and in-situ spectroscopic analysis. The computational analysis involves investigating the catalyst performance and interaction with $CO_2$ based on thermodynamics principles. Although computational analysis can provide useful insights into the reaction mechanism and catalyst performance, the best catalyst should not only be identified based on the computational analysis, but also by considering the electrochemical activation barriers and reaction kinetics [30]. Electrokinetics involves the investigation of $CO_2$ ECR through constructing Tafel plots [27]. While in-situ spectroscopic analysis yields mechanistic insights into the ECR process and enables samples analysis directly until the system reaches equilibrium [31]. The $CO_2$ ECR is a multi-electron and multi-proton transfer process. To date, the mechanism of $CO_2$ ECR is not fully well established, but it has been reported that $CO_2$ ECR into formate/formic acid occurs through four possible pathways as shown in Fig. 2.

The first pathway occurs through the formation of an intermediate that binds to the metal electrode through one or two oxygen atoms (Fig. 2A). Prior to that, the metal electrode forms a bond with hydrogen atoms through direct protonation with $H^+$ from the solution [32]. Another study reported the elimination of Hydrogen-metal bond formation and the direct oxygen-metal bond formation [33]. The second possible mechanism is the formation of carbon–metal bonds with the carbon that exists in carbon dioxide anion ($CO_2^{\bullet-}$)(Fig. 2B). Then, $CO_2^-$ is reduced through the protonation of the oxygen atoms and finally the intermediate is further reduced to HCOOH [34]. It is worth mentioning that this mechanism might also result in CO and $H_2O$ production instead of HCOOH. Fig. 2C shows a similar mechanism as Fig. 2B, but COOH is directly attached to the metal electrode instead of $CO_2^{\bullet-}$ intermediate. The last mechanism occurs at the tin oxide electrode, through $SnO_2$ reduction in a two-electron transfer process to form $Sn^{II}$ oxyhydroxide, which reacts with $CO_2$ to form surface-bound carbonate (Fig. 2D) [31]. Then, protons and electrons are transferred to the intermediate to form formate.

## 3. Factors affecting cell design

In this section, the main design factors that affect cell performance and cell operating parameters for $CO_2$ ECR to formate/formic acid are discussed. Fig. 3 summarizes the most significant factors that affect the cell performance.

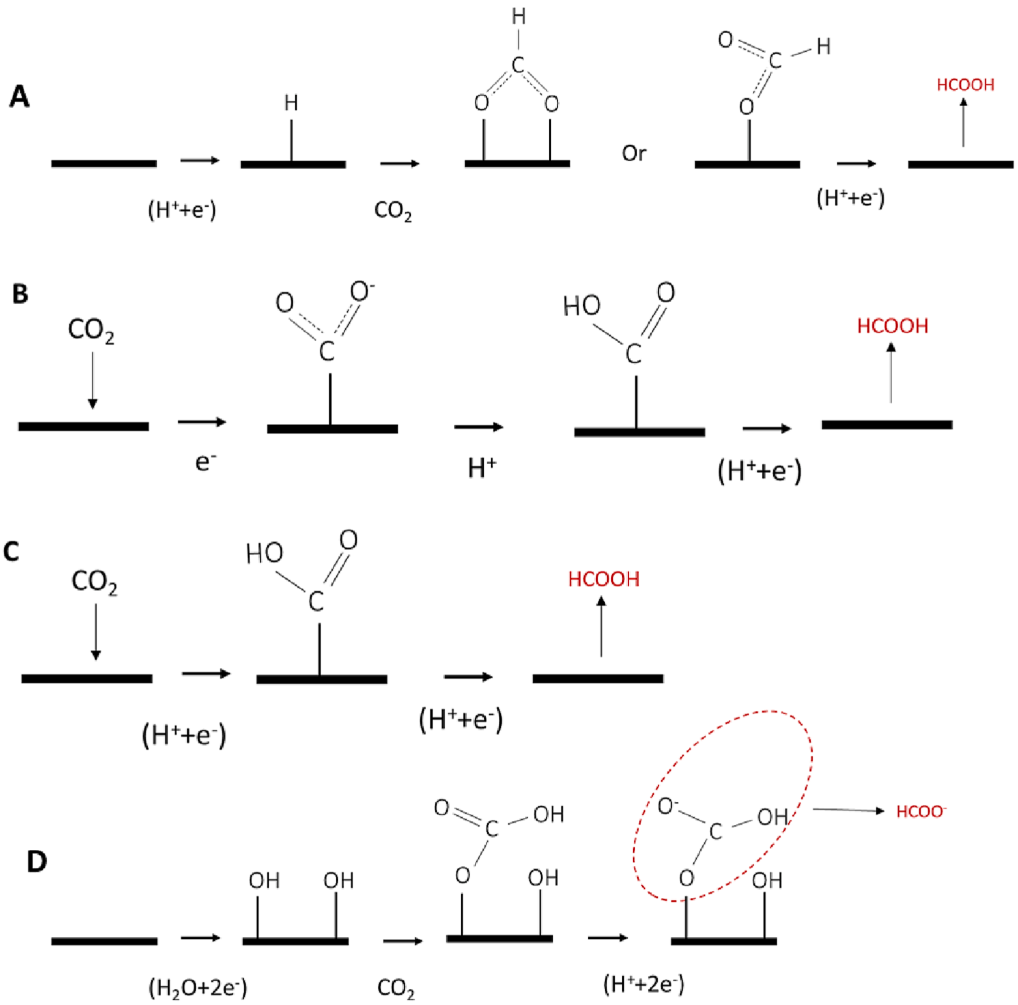

**Fig. 2.** Possible mechanisms for $CO_2$ ECR to formate/formic acid. (A) monodentate intermediate route, (B and C) $CO_2$– radical intermediate route, and (D) surface-bound carbonate intermediate route.

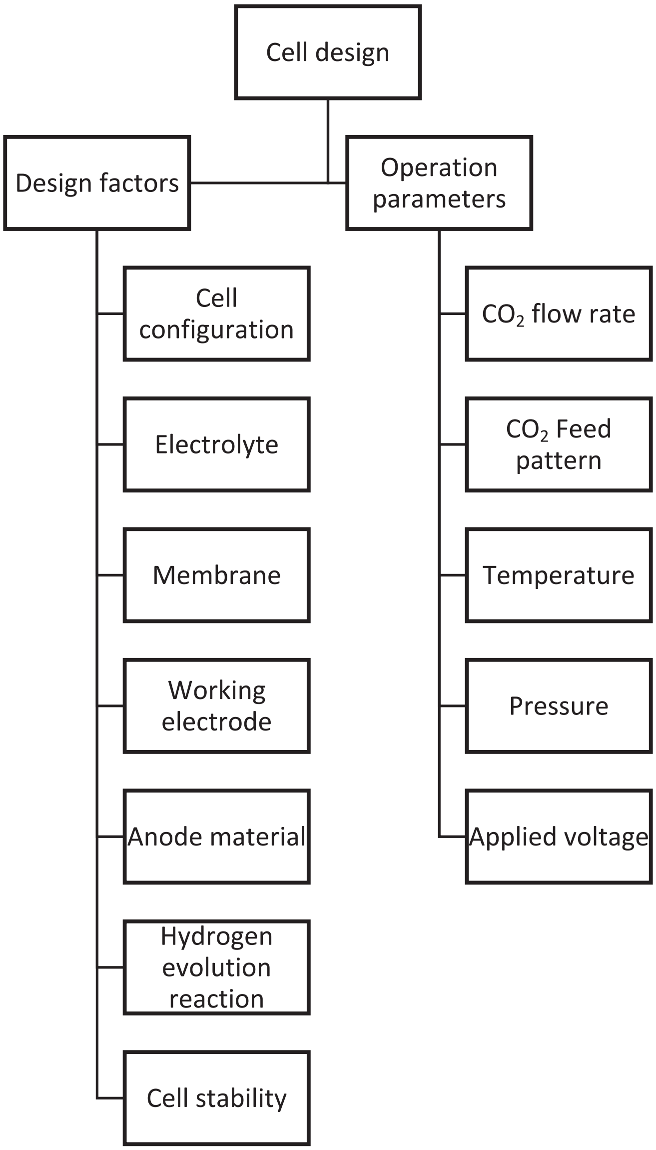

**Fig. 3.** The factors affecting the cell design.

### *3.1. Electrochemical cell design*

#### *3.1.1. Cell configuration*

*3.1.1.1. H-Type cell.* Several studies have utilized H-type cell for $CO_2$ ECR to formate/formic acid. There are three main structures of H-type cells reported in the literature: conventional, sandwiched, and the gas-tight H-type cell.

The **conventional H-type cell** consists of a cathodic compartment that contains the working electrode and the reference electrode, and an anodic compartment that includes the counter electrode. The working electrode is responsible for $CO_2$ ECR, while the counter electrode is an auxiliary electrode that is used to close the electric circuit. Electrodes are immersed in an electrolyte that is capable of transporting electric charge through the dissociation of ions. The two compartments are connected through a channel and separated by a membrane facilitating selective mass transport and preventing $CO_2$ ECR products (formate and formic acid) from oxidizing during the reaction [35]. The cathodic compartment is continuously fed with $CO_2$ gas to ensure electrolyte saturation and vented into a gas-sampling loop for gaseous products identification and quantification [3,36]. The $CO_2$ gas is often pumped for a certain duration (at least 30 min) to the reduction process to ensure electrolyte saturation and removal of residual air [37]. The reduction reaction is initiated by applying either an external voltage or current. This results in the formation of gaseous and liquid products, such as carbon monoxide and formic acid, respectively. The gaseous products are analyzed via Gas-chromatograph (GC) equipment with a thermal conductivity detector (TCD) for detecting hydrogen and a flame ionization detector (FID) for detecting carbon monoxide and other hydrocarbons [38]. The liquid products can be detected by ion chromatograph and/or proton nuclear magnetic resonance (NMR). Several authors tested various catalysts for $CO_2$ ECR to formate/formic acid in a conventional H-type cell (Table 1). Fig. 4a shows the general configuration of conventional H-type cell. In addition, a semi-batch H-type is used towards formate production in which the anolyte can be circulated, and the $CO_2$ is continuously pumped into the cathodic chamber (Fig. 4b).

One of the major drawbacks of H-type Cell is the limitation of $CO_2$ mass transport, which is due to the low solubility of $CO_2$ in aqueous electrolytes at ambient temperature and pressure resulting in poor $CO_2$ ECR [41]. Therefore, Qian et al. [42] suggested the use of a gas diffusion electrode (GDE) in a flow cell configuration in order to overcome such limitation. Löwe et al. [43] carried out a semi-batch experiment in H-type cell configuration using GDE to overcome the mass transport

**Table 1**
Performance for $CO_2$ electrochemical reduction into Formate/formic acid in H-type cell.

| Cell configuration | | Support material | Catalyst | Membrane | Electrolyte | Applied potential (vs. RHE) | Partial current density ($mA/Cm^2$) | FE% | Cell Stability (hr) | Ref. |
|---|---|---|---|---|---|---|---|---|---|---|
| H-type | H-Cell | Carbon paper | Sn | Proton exchange membrane | 0.5 M $NaHCO_3$ | −0.46 | 60 | 92 | 30 | [131] |
| | H-Cell | Carbon paper | Cu-Bi | Proton exchange membrane | 0.5 M $KHCO_3$ | −1.2 | 13 | 94.7 | 8 | [3] |
| | H-Cell | Carbon cloth | $SnO_2$ | Proton exchange membrane | 0.5 M $KHCO_3$ | −1.00 | 28.7 | 93.7 | 9 | [35] |
| | H-Cell | Carbon fiber | Cu-In hydroxide | – | 0.1 M $KHCO_3$ | −1.2 | ≈10 | 80 | 10 | [132] |
| | H-Cell | Glass carbon | N-doped porous carbon | Proton exchange membrane | 0.1 $NaHCO_3$ | −1.5 (vs. SCE) | – | 68 | 4 | [133] |
| | H-Cell | Copper foil | Sn | Proton exchange membrane | 0.1 M $KHCO_3$ | −1.08 | 8.5 | 97.8 | 10 | [35] |
| | H-Cell | Copper foil | Bi hexagonal sheet | Proton exchange membrane | 0.1 M $KHCO_3$ | −1.65 | – | 100 | 24 | [134] |
| | H-Cell | BiOI nanotubes | 2D bismuth oxoiodide | – | 0.5 M $KHCO_3$ | −0.90 | 31.1 | 97.1 | 65 | [135] |
| | H-Cell | Carbon paper | In-Sn | Nafion film | 0.1 M $KHCO_3$ | −0.98 | 236 | 86 | 58 | [136] |
| | H-Cell | Glassy carbon | Rod-like CuBi | Proton exchange membrane | 0.5 M $KHCO_3$ | −0.77 | – | 100 | 24 | [38] |
| | H-Cell | Copper | Cu@Bi nanocone | Naifon 117 membrane | 0.5 M $KHCO_3$ | −0.95 (vs. Ag/AgCl) | −31.9 | 96.9 | 10 | [137] |
| | Three electrode system | PANI/NF | Sn | – | 0.1 M $KHCO_3$ | −1.70 (vs. Ag/AgCl) | −19 | 94 | 10 | [138] |
| | Three electrode cell | Copper | Indium | Ion exchange membrane | 0.5 M $KHCO_3$ | −1.9 (vs. Ag/Ag/Cl) | −27.8 | 72.5 | 2 | [139] |
| | Three electrode system | Copper | Sn-CO | Ion exchange membrane | 0.5 M $NaHCO_3$ | −1.36 | 22.12 | 72.2 | 1 | [140] |
| | H-Cell | Carbon | Nanorod SnO | Proton exchange membrane | 0.5 M $KHCO_3$ | −0.7 | −60 | 94 | 1 | [42] |
| | H-Cell | Carbon | Indium | Proton exchange membrane | 0.1 M $Na_2SO_4$ | −0.71 | – | 96.5 | 1 | [141] |
| | H-Type | Carbon paper | Bismuth/reduced graphene | Proton exchange membrane | 0.5 M $KHCO_3$ | −1.17 | 28.1 | 92.1 | 30 | [142] |
| | H-type | Carbon cloth | Cu nanowires bridged Bi nanosheets | Cation exchange membrane | 0.5 M $KHCO_3$ | −0.86 | 14.6 | 87 | 8 | [143] |

(*continued on next page*)

Table 1 (*continued*)

| Cell configuration | Support material | Catalyst | Membrane | Electrolyte | Applied potential (vs. RHE) | Partial current density (mA/Cm$^2$) | FE% | Cell Stability (hr) | Ref. |
|---|---|---|---|---|---|---|---|---|---|
| Three electrode system<br>H-Cell | Lead<br>Carbon | –<br>Layered $Bi_2O_2CO_3$ | Anion exchange membrane<br>Proton exchange membrane | 1 M KHCO$_3$<br>0.1 M KHCO$_3$ | −1.0<br>−0.9 | −8.7<br>−0.73 | 48<br>90 | 160<br>100 | [144]<br>[145] |
| Gastight electrolytic cell | Carbon | Bi nanoparticles | – | 0.1 M KHCO$_3$ | −1.5 (vs SCE) | 14.4 | 92 | 20 | [146] |
| Gastight H-Cell | Carbon | CuO | Proton exchange membrane | 0.5 M KHCO$_3$ | −1.6 (vs. Ag/AgCl) | 14.3 | 65.1 | 20 | [147] |
| Gastight H-cell | Copper | Sn | Proton exchange membrane | 0.1 M KHCO$_3$ | −1.6 (vs. Ag/AgCl) | – | 95.6 | 55 | [37] |
| H-cell | Carbon fiber | $SnO_2/\gamma$-$Al_2O_3$ | Cation exchange membrane | 0.5 M KHCO$_3$ | −2.0 (vs. Ag/AgCl) | 21.7 | 65 | 152 | [127] |
| H-Cell | Copper | Sn/ γ-Al2O3 | Proton exchange membrane | 0.1 M KHCO$_3$ | −0.95 | 1.9 | 92 | 12 | [37] |
| H-Cell | Carbon paper | Pb/MWCNTs | Cation exchange membrane | 0.5 M KHCO$_3$ | −1.7 (vs. Ag/AgCl) | 28 | 84.6 | 10 | [148] |
| H-Cell | Copper | Bi | Proton exchange membrane | 0.5 M KHCO$_3$ | −1.7 (vs. NHE) | 23.34 | 91.46 | 5 | [113] |
| H-Cell | Membrane of the AgCl-SnO$_2$ precursor using polytetrafluoroethylene as a binder | $AgCl/SnO_2$ | Anion exchange membrane | 0.5 M KHCO$_3$ | −0.8 | 10 | 85 | 13.5 | [149] |
| H-Cell | Graphite | $Co_3O_4/CeO_2$ | Ion exchange Membrane | 0.1 M KHCO$_3$ | −0.75 (vs. RHE) | −6.1 | 76.4 | 45 | [150] |
| H-Cell | Sn-Pb-Sb foil | – | Ion exchange membrane | 0.1 M KHCO$_3$ | −1.4 | 8.3 | 91 | 16 | [151] |
| H-Cell | Graphene oxide | Sn foil-nitrogen doped | Ion exchange membrane | 0.5 M KHCO$_3$ | −1.0 | 21.3 | 92 | 20 | [152] |
| H-Cell | Titanium | $IrO_2/Ta_2O_5$<br>β-$PbO_2$/ | Cation exchange membrane | 0.5 M KHCO$_3$ | – | 12 | 40.2<br>22.2 | 24 | [39] |
| H-Cell | Carbon black | $In_2O_3$ | Proton exchange membrane | 0.5 M KHCO$_3$ | −0.9 | 29.5 | 87.6 | 12 | [153] |
| H-Cell | Carbon paper | Nanoporous-Sn/$SnO_2$ | Proton exchange membrane | 0.5 M NaHCO$_3$ | −1.1 | −16 | 80 | 58 | [154] |
| Three-electrode cell | Glass | Fluorine doped tine oxide | – | 0.1 M NaHCO$_3$ | −0.55 (vs. SCE) | – | 54 | 3.6 | [155] |
| H-Cell | Fluioride doped tin oxide | $Co_3O_4$ | Glass frit | 0.1 M TBAPF$_6$ in CAN + 1%vol H$_2$O | −1.5 (vs. NHE) | – | 27 | 8 | [156] |
| Three-electrode system | Copper foil | Pt/NCNFs | – | 0.1 M KHCO$_3$ | −0.6 | 46 | 93 | 50 | [157] |
| H- cell | Carbon paper | $SnO_2/CuO$ | Cation-exchange membrane | 0.5 M KHCO$_3$ | −1.0 (vs. SHE) | 24 | 74.1 | 30 | [158] |
| H-Cell | Glassy carbon | (di-halogen bismuth oxyhalide | Cation-exchange membrane | 0.5 M KHCO$_3$ | −1.6 (vs. SCE) | 0.7 | 98.4 | 14 | [159] |

(*continued on next page*)

**Table 1** (*continued*)

| Cell configuration | Support material | Catalyst | Membrane | Electrolyte | Applied potential (vs. RHE) | Partial current density (mA/Cm$^2$) | FE% | Cell Stability (hr) | Ref. |
|---|---|---|---|---|---|---|---|---|---|
| H-Cell | Copper | Nanostructured Bi | Proton exchange membrane | 0.1 M $KHCO_3$ | −0.6 | – | 100 | 10 | [160] |
| Three electrode system | copper | Bi | – | 0.1 M $KHCO_3$ | −1.5 | – | 91.3 | 9 | [161] |
| H-Cell | Carbon fiber | In-Sn | Cation-exchange membrane | 0.1 M $KHCO_3$ | −1.2 | 15 | 92 | 22 | [162] |
| H-cell | Carbon | Nitrogen doped tin oxide | Proton exchange membrane | 0.5 M $NaHCO_3$ + 0.5 M NaCl | −0.65 | 4 | 90 | 1 | [76] |
| H-Cell | Reduced graphene oxide | $SnS_2$ | Glass frit | 0.5 M $NaHCO_3$ | −1.4 | 11.75 | 84.5 | 12 | [76] |
| H-Cell | Carbon paper and carbon black with weight ratio 2:3 | SnO2 | Proton exchange mmebrane | 1 M $KHCO_3$ | −0.96 | – | 76 | 12 | [163] |
| H-cell | Glass | Copper modified palladium nanoparticles | Anion exchange membrane | 0.5 M $NaHCO_3$ | Over potential 0.15 V | – | 84 | 10 | [164] |
| H-cell | Carbon paper | Bi | Proton exchange membrane | 0.5 M $KHCO_3$ | −1.45 (vs SCE) | 18.9 | 90 | 20 | [165] |
| H-cell | Copper | Cd film | Proton exchange membrane | 0.5 M $KHCO_3$ | −1.8 (vs Ag/AgCl) | 10.6 | 76.2 | 5.5 | [109] |
| H-Cell | Carbon | Nanocubic $In(OH)_3$ | membrane | 0.5 $K_2SO_4$ | −1.1 | 5.2 | 77 | 7 | [166] |
| H-Cell | Carbon paper | $SnO_2$ | Proton exchange membrane | 0.5 M $KHCO_3$ | −1.7 (vs SHE) | 25 | 56 | 28 | [167] |
| H-Cell | Carbon paper | $SnO_2$ | Cation exchange membrane | 0.5 M $KHCO_3$ | −1.7 (vs SHE) | 12 | 62 | 12 | [168] |
| H-Cell | Copper | Sn | Proton exchange membrane | 0.1 M $KHCO_3$ | −1.4 (vs SHE) | 15 | 91 | 5 | [169] |
| Undivided three electrode cell | Copper | Sn | – | 0.1 M $KHCO_3$ | −1.8 (vs Ag/AgCl) | 8 | 83.5 | 4.5 | [170] |
| Three-electrode system | Carbon black | $SnO_2$ | – | 1 M KOH | −1.27 | 251 | 80 | 1 | [171] |
| High pressure- Semi continuous batch electrochemical reactor | Sn plate | – | Bipolar membrane | $K_2SO_4$ | 3.5 | 30 | 80 | – | [86] |
| H-type | Graphite | Pdpt | Proton exchange membrane | 0.1 M $K_2HPO_5$/0.1 M $KH_2PO_4$ | −0.4 | 5 | 88 | 2 | [172] |
| Rotating disk in three electrode system | Glassy carbon | Copper(I) oxide | – | 0.5 M $KHCO_3$ | −0.8 | – | 66 | 1 | [173] |

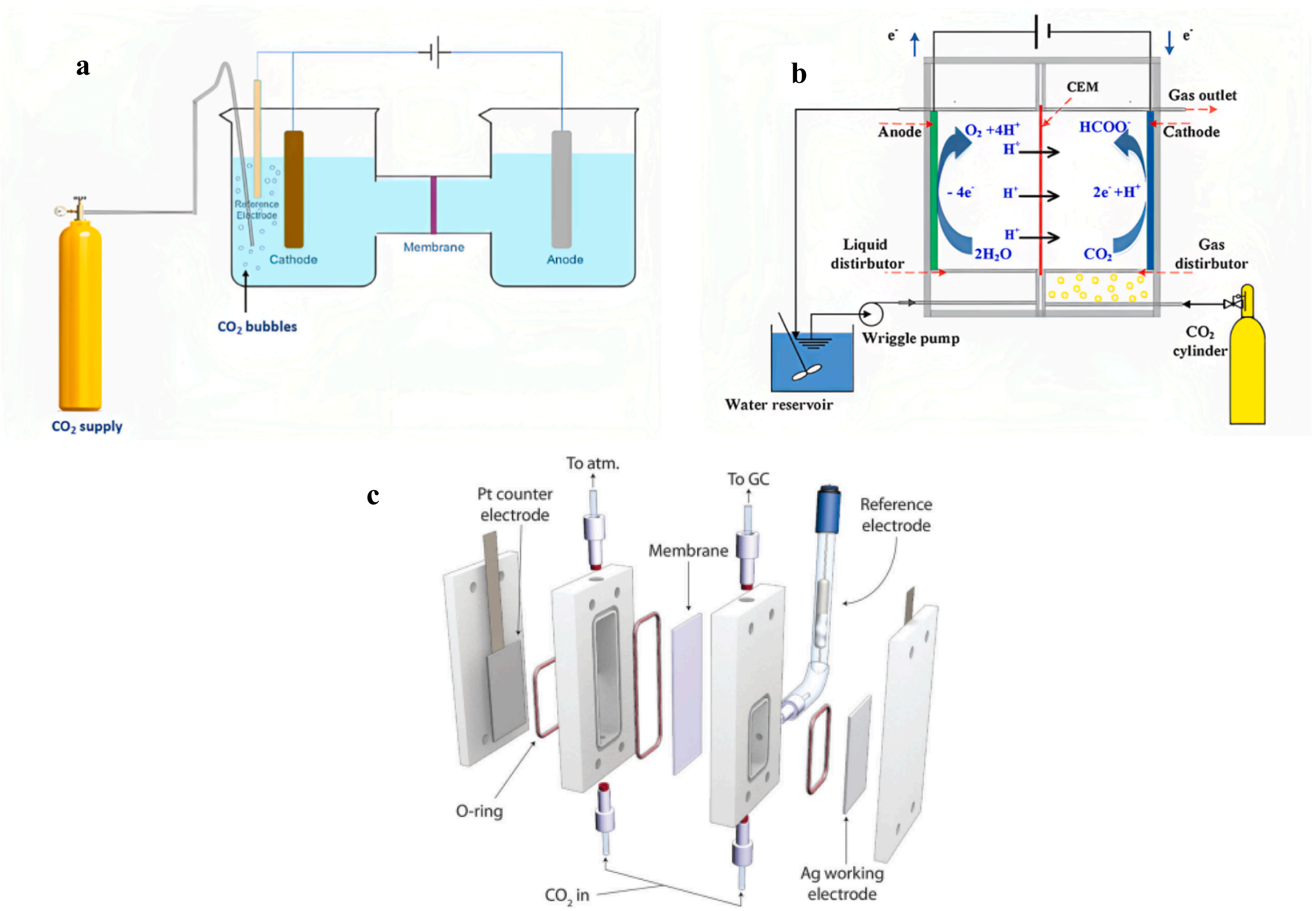

**Fig. 4.** (a) Conventional H-type cell configuration adapted with permission from [11] (b) conventional semi-batch H-type cell adapted with permission from [39] (c) the configuration of Sandwich H-type cell adapted with permission from [40].

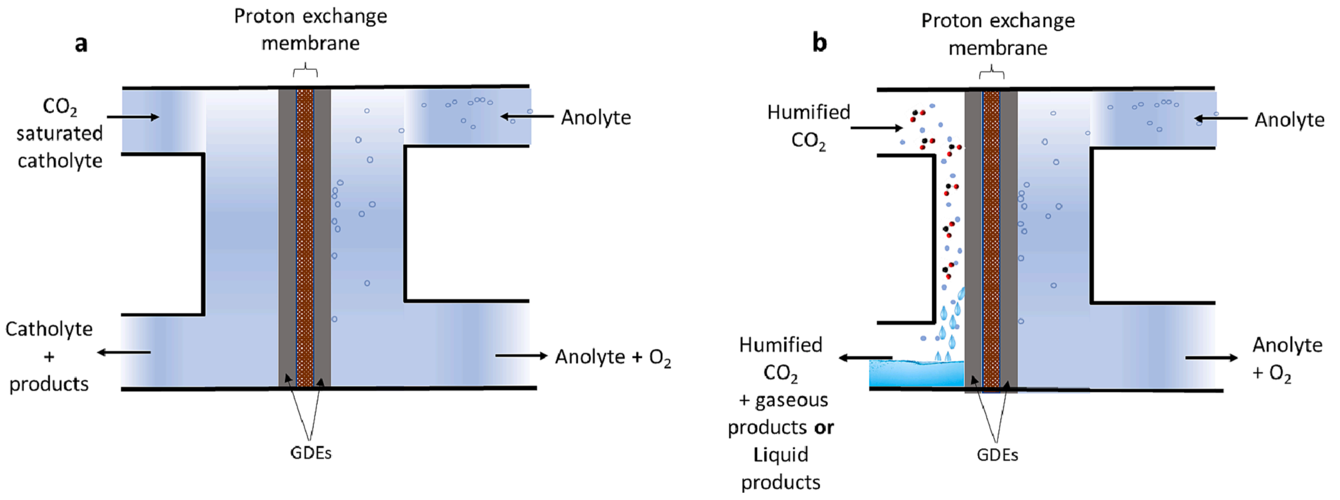

**Fig. 5.** PEM cell configuration (a) liquid phase $CO_2$ feed (b) gas phase $CO_2$ feed.

limitation and reported that the use of GDE (Section 3.1.4) alleviated $CO_2$ solubility issue that is caused by the temperature increase. The authors ascribed this to the short diffusion paths of dissolved $CO_2$ from the gas–liquid interference to the catalyst. Therefore, the use of GDE in H-type cell can effectively enhance the cell efficiency. The solubility of $CO_2$ can be increased by reducing the temperature or increasing the pressure; however, this is difficult to apply in conventional H-type cell. In order to increase the $CO_2$ solubility to overcome the $CO_2$ mass transport limitation, Kas et al.[44] suggested increasing the applied $CO_2$ pressure. The study highlighted that increasing the $CO_2$ pressure from 1 atm to 9 atm increased the formic acid FE from 3.52% to 20.80%.

It is worth mentioning that one of the significant limitations of H-cell is the low formate FE at lower aqueous pH of 3–5 compared to higher pH of 7–11. This is mainly due to the dominance of the hydrogen evolution reaction at low pH. Consequently, the cell produces alkali metal formate salts, which require an acidification process to produce formic acid.

Another challenge in using conventional H-type cell configuration is the low concentration of produced formate/formic acid in a large electrolyte volume and small electrode size, which might be difficult to detect. To mitigate that, Kuhl et al. [45] suggest a modified structure of H-type cell called **Sandwich H-type,** Fig. 4c**,** that accounts for a large electrode size and low electrolyte volume. This increases the concentration of formate/formic acid in the electrolyte resulting in a higher sensitivity in quantifying formic acid through the analysis technique. As can be seen, the working electrode is fixed in a parallel position to the counter electrode, and an anion exchange membrane is placed between the two compartments to prevent the reoxidation of the $CO_2$ ECR products (formate and formic acid). $CO_2$ gas flows within the cell and both compartments are filled with the electrolytic solution. Hatsukade et al. [40], investigated the $CO_2$ ECR on metallic silver electrode in a sandwich H-type cell. The study revealed that $H_2$ and CO are the major products reaching a maximum FE of 90%, while formate is a minor product reaching a maximum FE of 7%. It is worth noting that, the performance of this type of cell can be enhanced by using a catalyst that has high formate FE such as tin-based catalysts.

### *3.1.1.2. Flow cell*

*3.1.1.2.1. Polymer electrolyte membrane flow cell.* Unlike H-type cell, polymer electrolyte membrane (PEM) is a practical reactor for $CO_2$ ECR that can be used on an industrial scale. There are two main types of PEM cell configuration as shown in Fig. 5. Generally, a membrane is placed between the cathodic and anodic compartments to prevent the products crossover. In Fig. 5a, the membrane is sandwiched between electrolytes solution and in each compartment, a GDE is used (not necessary in the anodic side), and $CO_2$ is introduced in gaseous phase, whereas catholyte is introduced in liquid phase. While in Fig. 5b, the membrane is sandwiched between GDEs and the fluid flows in the backside (the so called zero gap arrangement) and the $CO_2$ is introduced as $CO_2$ gas or $CO_2$ humidified gas through the GDE [46]. However, the anodic compartment is fed with liquid electrolyte only. Furthermore, the use of GDE in PEM cells suppresses the mass transport limitation allowing a higher concentration of $CO_2$ in the cathodic compartment, which increases the reaction rate, and the cell efficiency.

The main advantage of the PEM cell is the high FE, continuous operation, ability to scale up without any reduction in the FE, and low internal resistance. However, the electrolyte and the membrane should be selected properly to achieve high FE and low internal resistance. In addition, similar to H-type cell, the electrolyte has a significant effect of the pH. This implies that any reduction of the pH below the allowed range will result in a hydrogen evolution reaction resulting in a lower formate FE [47,48].

Yang et al.[48] proposed a structure of PEM cell that can effectively modify the GDE structure resulting in a higher cell performance, reduced liquid flooding, and a stable pH of around 7–11 near the GDE so it can suppress the hydrogen formation. The proposed structure involves the use of an acidic center compartment, where formate is directly converted to formic acid. Fig. 6 shows the configuration of the proposed PEM cell. The cell consists of three compartments: anodic, center, and cathodic compartments. The center compartment is sandwiched between a cation membrane from the anodic side and an anion membrane from the cathodic side. The center pH is maintained between 1 and 5 using a strong acidic-ion exchange bead electrolyte. The anodic compartment is more acidic than the center compartment by allowing zero space with the anode. The pH is maintained between 7 and 11 near the GDE. The membrane in the anodic compartment (cation membrane)

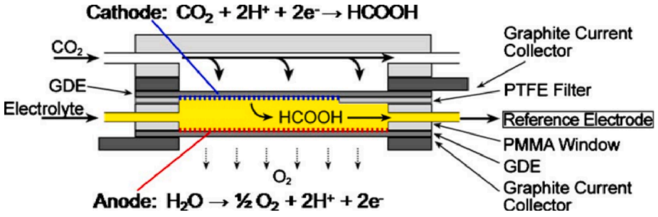

**Fig. 7.** microfluidic flow cell configuration adapted with permission from [49].

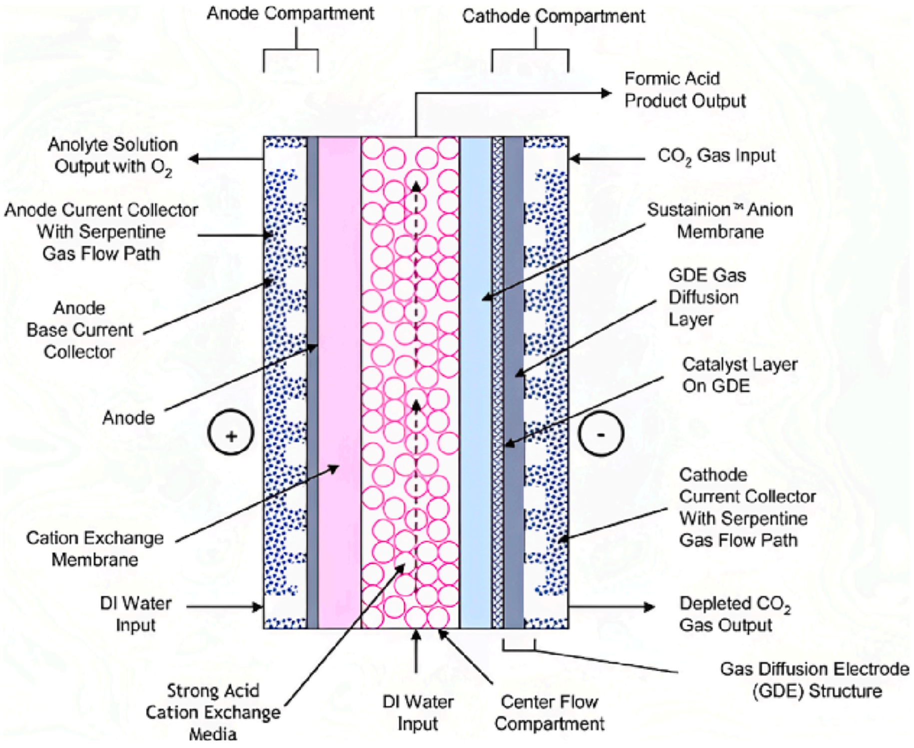

**Fig. 6.** modified PEM cell configuration adapted with permission from [48].

**Table 2**
Performance for $CO_2$ electrochemical reduction into Formate/formic acid in flow cell.

| Cell configuration | | Support material | Catalyst | Membrane | Electrolyte | Applied potential (vs. RHE) | Partial current density ($mA/Cm^2$) | FE % | Cell Stability (hr) | Ref. |
|---|---|---|---|---|---|---|---|---|---|---|
| Flow cell | Polymer electrolyte membrane | Carbon cloth | $SnO_2$ | Proton exchange membrane | 1 M KOH | −1.18 | 174.86 | 93 | 9 | [35] |
| | Polymer electrolyte membrane flow cell | Carbon paper | In-Sn | Anion exchange membrane | 1 M KOH | −0.98 | 236 | 94 | 58 | [136] |
| | Polymer electrolyte membrane | Troy paper | In/pb | Alkaline polymer membrane | 1 M $NaHCO_3$ | – | 40 | 80 | 1 | [47] |
| | Polymer electrolyte membrane | Sn foil | $SnO_2$ | – | 1 M KOH | −1.4 | 285 | 96.4 | 10 mintues | [174] |
| | Polymer electrolyte membrane | Carbon | $Sn_3O_4$ | Anion exchange membrane | 0.1 M $KHCO_3$ | −1.02 | 421 | 91.1 | 2.5 | [41] |
| | Polymer electrolyte membrane | Carbon | Nanorod SnO | Proton exchange membrane | 1 M KOH | −0.7 | −330 | 94 | – | [42] |
| | Polymer electrolyte membrane | Carbon paper | Sn nanoparticles | Ion-exchange membrane | 0.5 M $KHCO_3$ | 2.85 | 50 | 90.1 | 2 | [175] |
| | Polymer electrolyte membrane | Titanium | As-deposited Bi films | Proton exchange membrane | 0.5 M $KHCO_3$ | −0.82 | −1.6 - −8.3 | 75 | 6 | [176] |
| | Polymer electrolyte membrane | Toray paper | Sn/MWCNTs | Proton exchange membrane | DI water | 3.5 | 140 | 94 | 500 | [48] |
| | Microfluidic | Toray carbon paper | RuPd/Sn | – | 0.5 M KCl + 1 M HCl | −0.55 | 100 | 89 | – | [49] |

is used as the electrolyte. In addition, $CO_2$ flow into the GDE in the cathodic compartment, where it reacts with water coming from the center compartment to form formate ions. In the anodic side, water is oxidized into protons and oxygen. The generated protons flow to the center compartment through the cation exchange membrane. Similarly, the formate ions flow to the center compartments through the anion membrane. In the center compartment, formate reacts with protons to form formic acid. A 9.2 wt% formic acid is generated with a FE of 81%. Furthermore, the cell showed a good stability over 500 h.

*3.1.1.2.2. Membraneless (microfluidic) flow cell.* Membraneless or microfluidic flow cell was first proposed by Whipple at el. [49]. The cell consists of two GDE separated by a flowing electrolyte stream in which its pH and composition can be easily tolerated. $CO_2$ is fed to the cathodic side in which it is reduced directly to formic acid, while oxygen is released from the anodic side. The formic acid is directly removed from the system by the movement of the electrolyte. The reference electrode is placed in the electrolyte existing point or it can be placed in the electrolyte flow channel. It is worth mentioning that the gases produced within the cell are washed away by flowing electrolyte and/or escape from GDE. Fig. 7 shows the configuration of membraneless flow cell. In the same study, Whipple et al. investigated the cell performance using Sn catalyst at different pH. The results revealed that as the pH decreases the formic acid current densities and FE increase indicating an improved reaction kinetics. However, the pH could not be reduced less than 3 due to the catalyst instability. The maximum formic acid FE and current density were 89% and 100 $mA/cm^2$, respectively.

Wang et al.[50] developed a model for membraneless flow cell to study factors that significantly affect the cell performance for formic acid production. The study revealed that the main limiting factors are the $CO_2$ low diffusivity in the porous electrode, hydrogen evolution reaction at the cathode and hydrogen dilution effect. The results showed that GDE is responsible for the major mass transport resistance, which is mainly because of the steeper gradient in $CO_2$ concentration inside the GDE. In addition, the accumulation of $H_2$ gas near the reactive surface inside the GDE causing the dilution of $CO_2$ concentration and additional overpotential, which reduces the cell performance. Furthermore, the study mentioned that reduction of channel length can enhance the current density, which is due to the reduction in the concentration boundary layer thickness. However, the $CO_2$ utilization will be reduced due to the low $CO_2$ residence time in which there is no sufficient time for $CO_2$ to react with the electrode reactive surface. Table 2 shows the performance of $CO_2$ electrochemical reduction into formate/formic acid in flow cell.

Overall, the main advantage of this configuration is the ability to

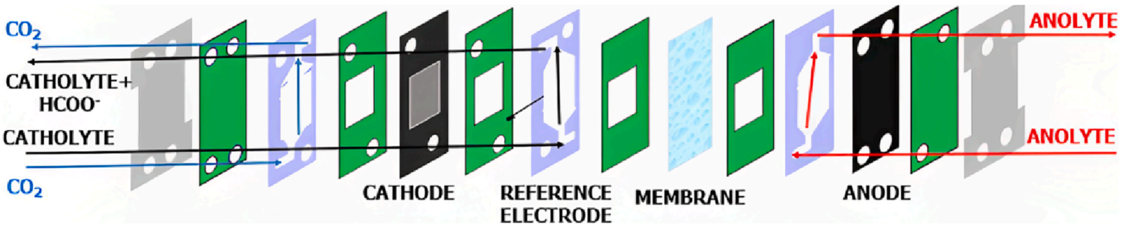

**Fig. 8.** filter press cell configuration adapted with permission from [52].

**Table 3**
Performance for $CO_2$ electrochemical reduction into Formate/formic acid in filter press cell.

| Cell configuration | Support material | Catalyst | Membrane | Electrolyte | Applied potential (vs. RHE) | Partial current density (mA/$Cm^2$) | FE % | Cell Stability (hr) | Ref. |
|---|---|---|---|---|---|---|---|---|---|
| Filter press | Carbon | Bi | Ion exchange membrane | 0.5 M KCl + 0.45 M $KHCO_3$ | −3.1 (vs. Ag/AgCl) | 90 | 49.5 | 1.5 | [52] |
|  | Carbon | Sn nanoparticles | Proton exchange membrane | A M KOH | −1.5 | 150 | 70 | 1.5 | [177] |
|  | Tin | Pb | Cation exchange membrane | 0.45 M $KHCO_3$ + 0.5 M KCl | −1.86 (vs Ag/AgCl) | – | 71.4 | 1.5 | [51] |
|  | Carbon paper | Sn particles | Ion exchange membrane | 0.45 M $KHCO_3$ + 0.5 M KCl | −2.0 (vs Ag/AgCl) | 90 | 70 | 1.5 | [178] |

carry out a continuous operation, electrolyte characteristics can be easily manipulated, high formic acid FE and the electrolyte flow can minimize the water management issues at the electrode including flooding or dry-out. However, as mentioned above, several factors limit the cell potential resulting in low formic acid production. The reasons behind these factors need to be experimentally studied and enhanced to achieve a high cell performance.

*3.1.1.2.3. Filter press cell.* Filter press cell or parallel-plate cell allows the operation of a continuous process in which both catholyte and anolyte pass once through the cell. Some research papers refer to the filter press cell as a special type of microflow cell [51,52]. The cell is divided into two compartments and separated by a membrane. An anolyte is fed into the anodic compartment, whereas the catholyte and $CO_2$ are fed into the cathodic compartment. $CO_2$ is initially pumped into the catholyte and then the solution is pumped to the filter press cell using a peristaltic pump. The existing anolyte is reserved in a tank; Similarly, the catholyte and liquid products are stored in a tank to be analyzed. In addition, GDE is usually used because it has larger electroactive surface area compared to other electrodes. For this type of cell, there is a growing interest in optimizing the cell performance using Sn GDE compared to others due to its superior performance compared to Pb GDE [51,53]. Fig. 8 shows all the components of a filter press cell.

Castillo et al. [52], investigated the effect of current density (j) and electrolyte flow per surface area (Q/A) on the performance of filter press cell for $CO_2$ ECR to formate using Bi GDE. The results revealed that increasing the current density j from 90 mA/$cm^2$ to 300 mA/$cm^2$ at Q/A of 0.57 mL.(min.cm)$^{-1}$ increased the average formate concentration from 2.04 g/L to 5.20 g/L; however, the FE reduced from 92.4% to 70.6%. The study highlighted that despite the reduction in FE, the formate rate doubled when the j was 300 mA/$cm^2$, which is beneficial to the process. Additionally, there was a significant increase in energy consumption from 177 kWh.kmol$^{-1}$ to 410 kWh.kmol$^{-1}$. Moreover, when the Q/A decreased from 0.57 mL.(min.cm)$^{-1}$ to 0.15 mL.(min.cm)$^{-1}$ at the same j (90 mA/$cm^2$), there was a significant increase in the formate concentration (from 2.04 g/L to 7.51 g/L) and slight increase in the energy consumption (from 177 kWh.kmol$^{-1}$ to 186 kWh.kmol$^{-1}$). Overall, it is required to achieve high formate concentration, FE, and energy efficiency towards formate with the possible lowest energy consumption for commercial-scale application. Table 3 shows the performance of $CO_2$ electrochemical reduction into formate/formic acid in filter press cell.

Thus, the cell configuration plays important role in the cell performance in which it affects the mass transport efficiency, process scale-up capability and operation sustainability. This eventually, affect the overall formate/formic acid FE and concentration as well as cell energy consumption. Considering the above discussion on the cell architecture, H-cell suffers from mass transport limitation, low liquid product concentration (due to small electrode size and large electrolyte volume), and electrolyte pH control. These limitations make H-type cell suitable for the performance evaluation of electrocatalyst prior to electrocatalyst utilization in flow cells. Even though sandwich type H-cell facilitated the quantification of low product concentration by using high electrode surface area in a low electrolyte volume, still the mass transport limitation pauses a challenge. This problem is suppressed in the flow cell (both PEM and Membraneless). In addition, high formate/formic acid FE and concentration can be generated in flow cell architecture using the catalyst that is highly selective towards these products. Furthermore, flow cell can effectively operate continuously with low internal

**Table 4**
Summary of different cell configuration performance towards formate/formic acid production.

| Cell configuration |  | Advantages | Disadvantages |
|---|---|---|---|
| **H-type** | **Conventional** | • Suitable for catalyst testing.<br>• Easy to operate. | • Poor mass transfer.<br>• Difficult to control temperature and pressure.<br>• Low formate/formic acid concentration.<br>• Not suitable for industrial application. |
|  | **Sandwiched** | • Low electrolyte volume<br>• Easy to quantify formic acid due to its high concentration. | • The configuration is restricted to flat shape electrode. |
| **Flow cell** | **Polymer electrolyte** | • Can operate with liquid catholyte or humidified $CO_2$.<br>• Allow zero-gap arrangement, which might result in better $CO_2$ conversion efficiency.<br>• Continuous operation.<br>Low internal resistance<br>• Can be scaled up without a reduction in the FE.<br>• Stable operation.<br>Allow the direct conversion of formate to formic acid during operation. | • The pH should be carefully controlled.<br>• Flooding of GDE with liquid electrolyte.<br>• Resistance due to the existence of the membrane.<br>• Membrane re-usability and cost. |
|  | **Microfluidic** | • Does not require use of membrane.<br>• Continuous operation.<br>• Electrolyte characteristics can be easily controlled.<br>• Reduced water flooding and dry-out issue. | • Accumulation of hydrogen gas near the cathode.<br>• Steep $CO_2$ gradient, which increases the mass transport resistance.<br>• Electrolyte flow rate should be carefully controlled.<br>• Relatively high energy requirement. |
| **Filter press cell** |  | • Continues operation.<br>• High formate production rate can be achieved. | • Relatively high energy consumption.<br>• Restricted to flat shape electrode. |

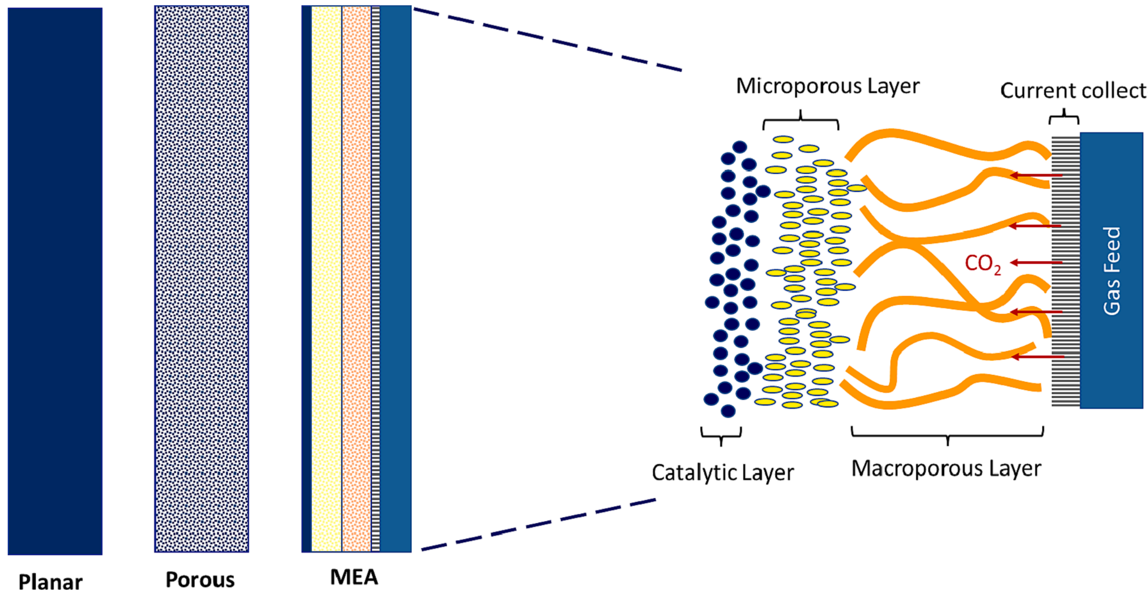

**Fig. 9.** The structure of planar, porous and MEA electrodes.

resistance. These advantages increase the flow cell reliability for scale-up. However, still the limitation of pressure drops across the membrane for PEM and cell architecture (e.g. channel length) need to optimize. Filter press can effectively operate in a continuous mode in which the anolyte and catholyte pass through the cell only once. However, the reusability of the electrolytes still needs to be investigated since they influence the process cost. Tables 4 summarizes the advantages and disadvantages of different cell configurations for formate/formic acid production.

### *3.1.2. Electrolyte*

The main role of electrolyte is to transfer charge between the electrodes and the catalyst during the $CO_2$ ECR process. The $CO_2$ can be directly pumped into the electrolyte or through the GDE. In case $CO_2$ is pumped directly into the electrolyte, salts present in the electrolyte reduce the $CO_2$ solubility elevating the mass transfer limitation [54]. Therefore, the electrolyte concentration should be managed. However, this problem is suppressed in case $CO_2$ is diffused through GDE. This is ascribed to the creation of three-phase boundary layer where $CO_2$ contacts the electrolyte near the catalyst, which enhances the $CO_2$ ECR process. Furthermore, the electrolyte influences the HER, system stability activity, formate/formic acid production rate, cell energy efficiency, current density, local pH, faradic efficiency and product selectivity [55-57]. Consequently, electrolyte is an important factor that can render or facilitate the cell performance. Therefore, the electrolyte characteristics and properties should be carefully considered to maximize the cell performance. Electrolytes are categorized into aqueous and non-aqueous. The concentration of the electrolytes affects $CO_2$ solubility due to salt effect. As there is no general rule that defines the $CO_2$ solubility as the electrolyte concentration varies, studies should investigate the effect of varying the electrolyte concentration on the $CO_2$ reduction efficiency. For instance, in $NaHCO_3$ solution concentration of 0.1 mol/kg, the $CO_2$ solubility varies between 0.07 and 0.43 mol/$kg_{NaHCO3}$ under $CO_2$ pressure ranges from 0.3 −1.9 MPa, respectively, at a temperature of 313 K [58]. Another study reported $CO_2$ solubility of 0.05 mol/kg at temperature of 278.15 K in a concentration of 0.5 mol/kg $NaHCO_3$ Under ambient pressure [59].

*3.1.2.1. Aqueous electrolytes.* Aqueous electrolytes consist of salts dissolved in a solvent, commonly water, such as $Na^+$, $K^+$, $Cl^-$ and $HCO_3^-$. As shown in Table 1, aqueous electrolytes are commonly used in $CO_2$ ECR into formate/formic acid owing to their high electroconductivity in water, which facilitates the $CO_2$ ECR process. The aqueous electrolytes consist of cations and buffering anions or non-buffering anions. In most studies dedicated to $CO_2$ ECR to formate, $KHCO_3$ is widely used and well known for its high performance [60,61]. This is because $KHCO_3$ can excessively provide the reactant ($CO_2$) for the reduction process at a potential more negative than −1.8 V vs SCE leading to high faradaic efficiency. Wu et al. [55] studied the effect of $KHCO_3$, $K_2SO_4$, and KCl on the selectivity and activity of Sn electrode for formate production. The results showed that $KHCO_3$ can provide sufficient local dissolved $CO_2$ to the interface between the electrode and the electrolyte. This is indicated by its stable current density over time. On the other hand, KCl and $K_2SO_4$ showed a reduction in the current density value over time indicating that the current density was limited by the diffusion of dissolved $CO_2$. In addition, $KHCO_3$ attained the highest formate production rate at a potential of −2.0 V vs. SCE compared to KCl and $K_2SO_4$. In fact $HCO_3^-$ has an important role in enhancing the formate/formic acid production rate. $HCO_3^-$ can provide an excessive amount of carbonaceous reactant, which enhances the $CO_2$ reduction process into formate/formic acid. In the same study carried out by Wu et al. [55] replacing $SO_4^{-2}$ with $HCO_3^-$ ion combined with $Na^+$, $K^+$ and $Cs^+$ resulting in a higher formate faradic efficiency by more than 10% at over potential less than −1.8 V vs. SCE. Also, the current density stability was enhanced over 60 min without a significant reduction. Besides, the formate production was enhanced by more than 200%. Even in the absence of an external $CO_2$ gas source, formate/formic acid can be generated in presence of $HCO_3^-$ ions [62]. Despite that, several research papers proved that $CO_2$ saturated electrolyte systems show poor formate FE and current density compared to gas-fed $CO_2$ system. This is justified by the fact that bicarbonates act as a substrate for the reduction process, and the poor performance is caused by the use of inappropriate cell configuration or catalyst. On the other hand, it is suggested that bicarbonates act as a carbon donor and $CO_2$ (supplied from the equilibrium reaction of bicarbonate with water) is the substrate for the reduction process. Yet, the main problem associated with bicarbonate that it also acts as a proton donor promoting the HER and resulting in a low formate FE [62-64]. In order to overcome this issue, recently, it was shown that by using cationic surfactants, HER is inhibited while $CO_2$ reduction ($CO_2R$) is promoted when using bicarbonate as feedstock [65]. Nevertheless, it is proposed that bicarbonates do not act as a proton donor and serve as a reactant that forms an intermediate that is directly reduced to form COOH intermediate [66].

Thereby, it is assumed that direct fed the GDE with $CO_2$ gas can increase the ECR cell performance through its direct contact with the electrocatalyst. However, there are some difficulties in collecting the liquid products such as ethanol and n-propanol through GDE. One of the main limitations is the liquid prod uct crossover through the GDE by evaporation. Highly volatile products with low production rate tend to have higher tendency to cross the GDE. Low volatile products like formate have more tendency to cross the exchange membrane rather than GDE through electro-migration [67,68].

Cations have a considerable effect on the formate/formic acid faradic efficiency, current density and production rate. The highest faradic efficiency and energy efficiency can be achieved using cations of order $Na^{+}>K^{+}>Cs^{+}$ using Sn and In electrodes [55,69]. It is worth mentioning that this order is in decreasing order of cation size, which indicates that larger cation size can achieve higher faradic efficiency. This is because at the same electrolyte concentration, large cations size attains to have a higher potential at OHP, which increases their electrostatic adsorption [55,70].

*3.1.2.2. Non-aqueous electrolytes.* Non-aqueous electrolytes including ionic liquids are also used for $CO_2$ ECR into formate/formic acid as shown in Table1. Non-aqueous electrolytes, especially ionic liquids are known for their enhanced $CO_2$ solubility compared to aqueous electrolytes, thereby suppressing the mass transport limitation and the competing HER. For instance, at 313 K under $CO_2$ pressure of around 0.7 MPa, the $CO_2$ solubility in aqueous $NaHCO_3$ is around 0.16 mol/$kg_{NaHCO3}$, whereas the $CO_2$ solubility in non-aqueous 30 wt% 2-(2-aminoethylamine) ethanol (AEEA) is around 10.99 mol/$kg_{AEEA}$ [58,71]. In addition, ionic liquids are used due to their electrical conductivity leading to enhanced $CO_2$ solubility [72] and production of high value chemicals such as oxalate [73]). However, non-aqueous electrolytes have low faradaic efficiency, which limits their industrial application. Consequently, ionic liquids can suppress HER due to their low proton concentration and reduces the overpotential for $CO_2$ ECR [74,75]. It is important to add water to the ionic liquid solution to prevent carbonate precipitation and enhance product distribution, which ultimately prevents any efficiency losses [76,77]. It is worth noting that there are some concerns associated with ionic liquids as electrolytes including preparation, price, toxicity and safety hazard [78,79].

*3.1.2.3. Electrolytes operation.* In liquid flow ECR cells, the electrolyte concentration is an important parameter that should be investigated as it links directly to the solution pH. In fact, the solution pH is the most critical factor that can enhance or diminish the ECR cell performance. This is because the solution pH would favor the HER over formate/formic acid at pH ranges other than the optimum range and affect the $CO_2$ solubility [80,81]. Formate is generally produced at pH neutral or slightly alkaline (below 10). The reduction of pH below the neutral conditions would favor the HER over formate production causing the formate FE to decrease. For instance, increasing the concentration of $KHCO_3$ solution from 0.1 M (pH 7) to 1 M (pH 7.8) causes the formate FE to reduce from 80% to 40% [81]. For formic acid production, mainly the optimized pH is around 4. In order to maximize the formic acid production relative to formate, the system should operate at pH below or at 3 [82]. However, this would damage the electrode structure, and increases the HER activity. Studies showed the highest formic acid FE of 70% was achieved at pH 4 [83], and 37% at pH 3.9 in KCl solution [84]. At pH lower than 4, the HER denominates due to the high proton concentration compared to the $CO_2$ concentration. This causes bubbles to cover the electrode surface, which increases the bubble overpotential and reduces the electrode efficiency. Nevertheless, even in a controlled pH environment, the local pH near the electrode's surface may deviate from the bulk's pH. This is ascribed to the production of $OH^{-}$ ions from the $CO_2$ reduction reaction (Eq. (1)) and HER (Eq. (2)). Yet, this effect is counteracted by the formation of bicarbonate buffer by $CO_2$ according to the reactions below and can be counteracted further by using buffer electrolytes.

$$CO_{2(aq)} + H_2O \leftrightarrow HCO_3^- + H^+ \tag{1}$$

Or.

$$CO_{2(aq)} + OH^- \leftrightarrow HCO_3^- \quad pH > 7 \tag{2}$$

The electrolyte flow rate is another important fluid dynamic factor that would affect the $CO_2$ ECR process. At ambient pressure, the formate/formic acid FE and current density increases as the flow rates increase up to an optimum value. This is because higher flow rate would (1) reduce the thickness of the diffusion boundary layer, which increases the $CO_2$ mass transfer to the electrode surface (2) increases the transfer of dissolved ions present in the electrolyte to the electrode active sites, which increases the conductivity and thereby enhances the reduction efficiency. Any increases in the catholyte flow rate beyond the optimum value would reduce the cell performance mainly due to the decline in residence time, excessive turbulence in the cathode chamber that affects the $CO_2$ absorption and production of dead zones across parts of the cathode. Also, at a low flow rate the poor performance could be attributed to the low $CO_2$ mass transfer, and insufficient ions supply including the $H^{+}$ and $OH^{-}$ that limit the formate/formic acid production. It is worth noting that at higher pressures (e.g. $>$ 15 bars), higher formate/formic acid FE and current density are obtained at a low catholyte flow rate. This is because $CO_2$ mass transfer is not the limiting factor at a higher pressure and the enhancement could be due to the high $CO_2$ solubility at a higher pressure and the improved proton transport to the cathode [85-87].

### 3.1.3. Membrane

In $CO_2$ ECR cells, membranes are commonly used to separate the anodic and cathodic compartments preventing the formate/formic acid to oxidize in the anodic compartment. The membrane allows the use of two different electrolytes with different pH conditions. However, not all cell configurations require the use of membrane as discussed in section 3.1.1 such as in microfluidic cells. In fact, the continuous movement of electrolyte that carries the formate/formic acid eliminates the need of using a membrane. As shown in Table 1, three main types of membranes are used in $CO_2$ ECR cell: cation exchange membrane (CEM), anion exchange membrane (AEM) and bipolar membrane (BPM). CEM is a monopolar membrane with a fixed negative charge in which it allows the cations to pass and prevent the passage of anions. Whereas AEM is a positively charged membrane that allows the passage of anions while rejecting cations [88-90]. BPM is a selective membrane towards anions and cations. It comprises a charged anion exchange layer and negatively charged cation exchange layer. AEM and CEM are cheap, easy to manufacture, stable and have long lifetime. However, they suffer from high product cross over, electrolyte contamination and high pH gradient across the membrane. It is worth mentioning that the formate crossover issue in AEM is much greater than CEM. Overall, these disadvantages can be overcome by using BPM. In fact, compared to AEM and CEM, BPM can effectively maintain a constant pH across the membrane through its selective transport of anions and cations. In addition, the products crossover and electrolyte contamination are minimized. However, BPM is expensive, has a short lifetime and suffers from low stability of the anion exchange layer. The short lifetime is mainly due to layers delamination that is caused by the accumulation of water on the interface due to bicarbonate crossover that converts to $CO_2$ resulting in membrane swelling [86,89,91,92]. Nevertheless, a recent paper highlighted that the use of alkaline anion exchange membrane combined with alkaline electrolyte (KOH) result on a better selectivity of formate by suppressing the HER besides the low solution resistance and confinement of free $CO_2$ gas that KOH provides [93].

The performance of CEM and BPM under similar conditions were investigated [87]. The results showed that the use of CEM membrane requires higher catholyte concentration, which is about 1 M $KHCO_3$ and 0.5 M $KHCO_3$ for CEM and BPM, respectively. In addition, at low pressure (e.g. 1 bar), ECR cell with BPM show higher format concentration and FE, and lower current density. Also, in ECR cell where CEM is used, it is recommended to use acidic anolyte. However, it is not recommended to use acidic anolyte with BPM because the current density and formate amount are reduced significantly compared to alkaline anolyte. Systems that involve the use of BPM require the use of alkaline anolyte. Despite that, it is not recommended to use bicarbonate as the anolyte since the bicarbonate ions will react with the hydroxide ions from the BPM to form carbonates. For the catholyte, it is recommended to use a neutral to slightly alkaline solution. In fact, it is preferred to use $KHCO_3$ as a catholyte as discussed in Section 3.1.2 [86]. It is important to mention that the cathodic compartment can operate without the use of liquid catholyte. In that case, water is supplied through the membrane from the anodic compartment [94]. In addition, the membrane thickness plays an important role in the energy requirements. As the membrane thickness increases, the ohmic drop increases and subsequently increases the cell voltages resulting in a high electricity requirement.

### 3.1.4. *Working electrode*

The reduction of $CO_2$ into formate/formic acid occurs at the working electrode (cathode) at pH around 7 and it is expressed as:

$$CO_2 + H_2O + 2e^- \rightarrow HCOO^- + OH^- \quad (3)$$

The formate anions combine with the positive ions that are transported from the anodic compartment through the membrane or positive ions available in the electrolyte.

Properties including the electrode geometry, shape, configuration, composition, porosity, and electrode material influence the electrode $CO_2$ reduction capability. There are three types of electrodes, which are planar, porous and membrane electrode assembly (MEA) as shown in Fig. 9. MEA consists of catalytic layer (CL), Microporous and Macroporous layer, current collector and gas feed.

Planar electrode is not commonly used due to its unreliability in $CO_2$ ECR cell [95]. On the contrary, MEA are used in two main configurations, which are GDE and Catalyst Coated membrane (CCM). Compared to planar and porous electrodes, GDE has lower mass transfer resistance and larger electroactive sites per unit area. GDE is fabricated by depositing the catalyst ink on a microporous layer of gas diffusion layer, mainly carbon support, Whereas CCM involves depositing the catalyst ink on a polymeric membrane [96]. In GDE, the support layer (microporous and microporous layer) is mainly made of porous materials that facilitate gas transport. The microporous layer is an optional layer that can enhance the $CO_2$ distribution over the catalyst layer. Carbon powder is commonly used as a microporous layer. Whereas the macroporous layer is mainly carbon-based material (e.g. carbon nanotubes and woven fabric carbon cloth) mixed with a hydrophobic polymeric material. Among the carbon support material reported, carbon nanotubes possess a high mass transfer rate, good stability and productivity, and more confinement of catalytic layer and $CO_2$ gas [97]. The main issue associated with carbon materials is that they can facilitate the HER. However, the hydrophobicity of the support can be enhanced to prevent HER by applying surface and structure changes, such as incorporating catalytic metal sites into the carbon structure (e.g. the metal organic frameworks (MOF) [98]. A recent study reported that the addition of binders, such as polytetrafluoroethylene (PTFE) enhanced the catalyst active surface area, the $CO_2$ diffusion channels around the active surface and reduced the HER resulting in enhanced formate production [99]. It is worth mentioning that the cathode microstructure governs the gas diffusion and the charge exchange and transfer, which influence the $CO_2$ reaction and subsequently influence the cathode performance [100].

The catalyst can be coated/deposited on the support through various methods including spraying, screen printing, rolling and electrodeposition. Spraying involves the spraying the electrocatalyst ink through a nozzle to form fine aerosols, whereas screen printing involves creating a stencil on a mesh screen followed by pushing the electrocatalyst ink through that stencil [101,102]. Rolling method involves sieving the electrocatalyst through a silver mesh onto a support or directly introducing the electrocatalyst to the support followed by passing the support loaded with electrocatalyst between two rollers [103]. In electrodeposition, an electrical current is used to reduce the cations existing in an electrolyte to form an electrocatalyst thin film [104]. It is worth mentioning that CCM electrode eliminate the need to use liquid catholyte and can effectively work in gaseous phase (humidified $CO_2$) catholyte. This eliminates problems including the low $CO_2$ solubility that limits the reaction rate and the occurrence of secondary reactions; yet the system is difficult to control. GDE can effectively overcome the mass transport limitation due to low $CO_2$ solubility in aqueous electrolyte by maintaining a high $CO_2$ concentration near the catalyst surface. In addition, GDE provides has a good mechanical stability, contributes to system stability, can operate at higher current densities (e.g. 200 mA/$cm^2$) and reduces ohmic losses and achieve higher formate production rate. Besides that, GDE prevents cathode flooding by providing a passage for byproducts removal due to its highly structured three-phase boundary [105,106]. For instance, Díaz-Sainz et al.[96] carried out a comparative study between GDE and CCM electrodes. For the same electrocatalyst, the study showed that CCM electrode outperform GDE in term of formate concentration, FE, and energy consumption per Kmol of formate. However, the formate production rate of CCM electrode was much lower than GDE, as low as 75% due to the low operating current density. The study highlighted that GDE is more suitable for operating at higher current density resulting in higher $CO_2$ reduction and formate production rates.

The formation of formate is governed by the local proton concentration in the reaction zone and the local electrical field. Therefore, as the thickness of the catalyst layer increases the current density increases, which subsequently increases local proton concentration resulting in higher formate FE. However, the local electrical field is reduced with the increase in the catalyst layer thickness, which impedes the formation of formate [107]. Another reason could be the limitation of reactants diffusion as the catalyst thickness increases, which reduces the formate FE. A study reported that at constant overpotential, as the thickness of the catalyst layer increase, the partial current density and faradaic efficiency towards formate increases up to certain metal loading. This is ascribed to the increase in the total area of three-phase boundaries. However, a further increase in the metal loading causes a reduction in the current density as well as the faradaic efficiency due to the reduction in reactants diffusion [108,109]. In addition, the increase in the catalyst layer thickness beyond the optimum thickness cause a shift in the product distribution (e.g. from formate to CO). A study reported that the thickness of the catalyst layer has a significant effect on the overpotential of the reaction at a constant current density, which might cause a shift in the product distribution. For instance, increasing the metal loading up to certain amount may increase the FE considerably. However, further increase in the metal loading leads to a significant reduction in formate FE causing the FE of other products to increase. For instance, at low metal loading of 5 mg/$cm^2$, the formate FE reached 93% at 50 mA/$cm^2$ requiring a higher reactor voltage. Yet, additional increase in the metal loading reduces the voltages, but the FE decreased significantly to 82% with a considerable rise in the CO FE [80]. It is worth noting that the cell voltage is the sum of equilibrium electrode potentials, overpotentials and potential drop across the electrolytes as well as the membrane. Moreover, the cell voltage is significantly influenced by the ohmic drops.

The type and the properties of the support layer also have an important effect on the $CO_2$ ECR to formate/formic acid. The support layer affects the $CO_2$, protons and electron transport within the catalyst layer as well as the HER activity, which subsequently influences the $CO_2$ ECR. As disused above, the type of support layer influences the HER activity, which influences the $CO_2$ ECR. For example, mesopores carbon (pore size 1.7–20 nm) has a higher capability towards HER suppression compared to activated carbon (pore size 1.7–60 nm) and acetylene black (pore size 17–50 nm) [5]. Generally, the primary pores (exist on the catalyst layer deposited on the support) acts as a reaction zone, whereas the macroporous layer acts as $CO_2$ gas channel. The primary pores surface area determines the cell performance towards formate production. As the primary pores surface area increases, the current density of formate increases leading to better cell performance. Han et al.[5] reported that the optimum pore size of the primary zone for the $CO_2$ ECR to formate ranges between 5 and 20 nm, which differs from the optimum pore size of other carbon-supported electrodes for $CO_2$ ECR to gaseous products (e.g. CO). In addition, for carbon support, the enhanced graphitic degree enhances the electron transfer, which subsequently enhances the $CO_2$ reduction reaction. Furthermore, the $CO_2$ adsorption capability and charge transfer capability of the support layer impact the electrode reduction performance. Therefore, these parameters should be studied in order to optimize the electrode performance.

The fraction of the support layer (microporous and microporous layer) plays a deceptive role in the electrode performance. The effect of increasing the support layer fraction on current density and formate production is similar to the effect of the catalyst layer thickness. As the thickness of the support layer increases the current density increases along with the formate FE due to the support layer microstructural evolution that increases the local proton concentration near the catalyst surface. However, further increase in the support layer fraction beyond the optimum thickness, the formate FE decreases due to the blockage of catalyst sites that subsequently reduces the gas permeability and increases the mass transport resistance.

In addition, the catalyst size influences the electrode performance towards $CO_2$ ECR process. Small catalyst size could lead to higher formate/formic acid yield [110]. However, it is also reported that the particle size of the electrocatalyst does not have an effect on the electrode performance under the optimum support layer and catalyst layer thickness. Wu et al. [107], highlighted that the formate production using Sn electrode with the optimized support layer fraction (Nafion) is independent on the Sn size that ranged between 100 nm and 2000 nm. Nevertheless, the thickness of the catalyst layer and support layer (Nafion) fraction affects the Sn electrode performance towards formate production significantly. The optimum catalyst thickness was about 9 μm, while the Nafion fraction was roughly 20 wt%. Therefore, the catalyst size does not define the performance of the electrode. Other factors such as primary zone pore size, primary pores surface area, electroactivity of the catalyst, primary zone $CO_2$ adsorption capability, support layer porosity, and support layer electron transfer capability have a direct influence on the electrode performance. Nevertheless, in order to achieve the optimum catalytic activity, the catalyst must demonstrate a high mesoporosity and 3D hierarchical structure. This results in a larger specific surface area and maximizes the contact surface area between the electrode and the electrolyte, which facilities fast mass transport as well as electro-transfer rate [111].

It is worth mentioning that the electrode fabrication methods parameters, such as annealing temperature and electrodeposition time influence the structure, superficial area, and the electroactivity of the catalyst. Furthermore, recent study showed that the type of precursor can influence the selectivity and the degree of alloy component formation. For instance, a recent study reported that the use of $SO_4^{2-}$ precursor in Cn/In/MOF electrocatalyst synthesis promoted the formation of In, which increased the catalyst stability, selectivity towards formic acid and FE compared to $NO_3^-$[112].Therefore, the fabrication parameters should be well optimized [113,114].

### 3.1.5. Anode material

The oxidation reaction occurs in the anodic compartment at pH 14 simultaneously with the reduction reaction at the cathode, and it is expressed as:

$$2OH^- \rightarrow \frac{1}{2}O_2 + H_2O + 2e^- \tag{4}$$

The electrolyte used in the anodic chamber (anolyte) could be water or other organic and inorganic electrolytes as mentioned in Section 3.1.2. Despite that, water dissociation occurs at both the cathodic and anodic chambers. Furthermore, in some cell configurations, the cathodic and anodic compartments are separated by a membrane to prevent formate/formic acid oxidation. Other configurations do not include the use of a membrane and the continuous movement of the electrolyte (e.g. membraneless flow cell) prevents formate/ formic acid oxidation. However, the existence of a membrane ensures maintaining the alkaline conditions to ensure oxygen evolution at low equilibrium potential for oxygen evolution reaction (OER) [87]. Besides that, it is important to reduce the oxygen evolution potential (OEP) at the anode as it reduces the electrical energy required for the $CO_2$ ECR and consequently increases the total cell energy efficiency [115]. The OEP is the major contributor to the cell voltage requirements by more than 50%. In addition, lower cell voltages enhance the formate production. This is because the production of formate involves the transportation of $H^+$ from the anodic to the cathodic compartment. As the OEP increases, the cell voltage increases, which strengthens the electric field intensity and enhances the $H^+$ transfer across the membranes to the cathodic compartment. However, $H^+$ reduction reaction is faster than formate generation reaction. Therefore, formate regeneration decreases and hydrogen evolution increases [39]. Most of the studies showed that noble metals and their oxides have excellent performance and good stability. Yet, the oxides are more stable since they cannot be further oxidized. To date, platinum (Pt) electrode is widely used in $CO_2$ ECR. It has been proven that the use of Pt cermet electrode reduced the anode overpotential and ohmic resistance while increased the $CO_2$ ECR reaction at the interfaces [116]. Nevertheless, its activity towards OER is limited due to the potential for oxide formation. Other studies showed that iridium oxide ($IrO_2$) outperforms other catalysts including Pt in term of cell performance and stability [117,118]. For instance, Jiang et al.[39] studied the effect of three anode material (Pt, $IrO_2$-$Ta_2O_5$/Ti, and β-$PbO_2$/Ti) on the performance of Tin cathode for $CO_2$ ECR to formate. The study showed that $IrO_2$-$Ta_2O_5$/Ti exhibited the highest FE and energy efficiency, and the lowest power consumption. It is reported that it reduced the cell energy requirement by 53.8%, which reduces the formate production price. In addition, $IrO_2$-$Ta_2O_5$/Ti electrode contained more active sites as well as less interfacial charge-transfer resistance, which accelerates the water oxidation process. However, noble metals are generally expensive and require neutral electrolyte for OER, which limit their applicability in large scale production.

The electrolyte affects the type of the anode that can be used. The use of alkaline electrolyte such as KOH can effectively reduce the anode cost. This can be achieved by utilizing highly reactive non-noble metals such as cobalt and iron as an OER catalyst rather than noble metals along with alkaline electrolyte. This combination can provide a good cell performance [119].

In undivided $CO_2$ ECR cells where the cathodic and anodic compartments are not separated, thereby formate can be oxidized on the anode causing the concentration of formate to decrease significantly. Generally, the three-electrode system is used to investigate the performance of catalysts as this system is not practical to implement in industry. However, there are ways to prevent or reduce the formate/ formic acid oxidation on the anode in an undivided three-electrode system. For instance, a study reported that coating the Pt electrode with Nafion membranes can reduce the oxidation rate of formate resulting in a higher formate concentration in the electrolyte compared to uncoated Pt anode [120]. This can provide better information regarding the catalyst performance towards formate production. The Nafion layer prevents the formate to reach the Pt surface, while it allows the water to pass. The addition of Nafion layer caused the formate concentration to increase to 0.12 mol.L$^{-1}$ compared to 0.023 mol.L$^{-1}$ for

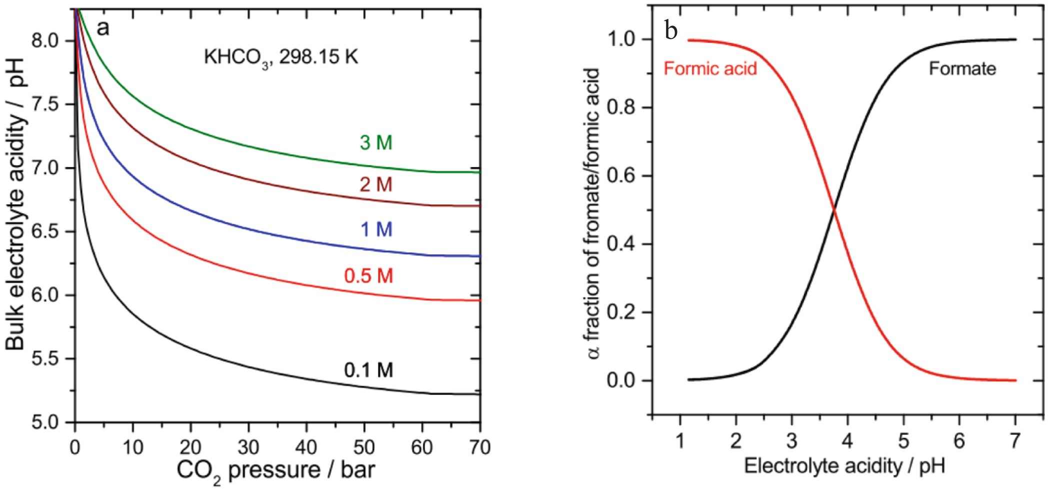

**Fig. 10.** (a) The effect of $CO_2$ pressure on the electrolyte pH at different electrolyte concentration (b) the distribution of formate and formic acid at different electrolyte pH at 25 ℃ adopted with permission from [82].

uncoated Pt electrode. In addition, as the Nafion content on the Pt electrode increased from 0% to 5% the faradaic efficiency increased from 38% to around 81%. Furthermore, in undivided cell, the dissolved Pt from the Pt electrode can act as a cathode contaminant causing carbon monoxide to be adsorbed on the catalyst surface leading to catalyst corrosion [121,122].

### 3.1.6. Hydrogen evolution reaction (HER)

The HER can reduce the cell efficiency towards formate/formic acid production by competing with the electrode reaction mechanism and dilution of $CO_2$. Therefore, it is important to suppress the HER in order to optimize the cell performance. This suggests that HER kinetics is one of the important cell parameters that need to be minimized. The HER typically occurs at current density between 0.01 mA/cm$^2$ and 1 mA/cm$^2$ in GDE and it is expressed as:

$$2H_2O + 2e^- \rightarrow H_2 + 2OH^- \quad (5)$$

Thermodynamics principles apply that HER occurs at cathode potential lower than −1.02 V vs. SHE. However, a recent study suggests that HER has minor effect on cell performance towards $CO_2$ reduction reaction at −1.02 V vs. SHE till the cathode potential drops to −2 V vs. SHE. This is because beyond −2 V vs. SHE, the partial current densities of $CO_2$ and $H_2$ overlap resulting in a lower energy efficiency and cell performance. As shown in Table 1, the optimum FE for formate production typically occurs at cathode potential −1.7 vs. SHE. Yet, several studies emphasize that the HER is still a challenge in $CO_2$ ECR into formate/formic acid cells [107]. The cell configuration influences the degree in which HER affects the cell performance. For instance, the HER has a significant effect in flow channel ECR cell structure (e.g. microfluidic cell). In flow channels, the $H_2$ concentration may increase along the channel, which accumulates inside the GDE near the reactive surface area causing $CO_2$ dilution and resulting in a lower cell performance [50].

Overall, the HER can be effectively suppressed by using a highly selective and active catalyst towards $CO_2$ formate/formic acid production. In addition, increasing the hydrophobicity of the macroporous and microporous layer suppresses the HER. Also, the use of proper cell dimension in some cell configuration such as microfluidic cell reduces the effect of HER. As discussed in Section 3.1.5 some anodic materials increase the cell voltages allow the passage of $H^+$ ion promoting the HER over formate.

### 3.1.7. Cell stability

One of the most important factors while designing the ECR cell is the long-term cell stability during operation. Cell stability is most likely influenced by the stability of electrode structure, catholyte type, phase and concentration, CL structure and membrane type. A stable $CO_2$ ECR cell showed an acceptable and stable formate/formic acid FE, current density and cell voltage. For industrial scale, the cell should demonstrate a stable performance for at least 8000 h per year [123]. It is well-established in the literature that the degradation and deactivation of the CL is the main reason responsible for the poor cell stability. This is ascribed to the catalyst poisoning and contamination by the metal impurities, intermediates, CO produced from the side reactions, and impurities in $CO_2$ gas. For instance, the use of industrial $CO_2$ purified gas might cause catalyst poisoning due to the presence of small quantities of $H_2S$. However, CuSx catalyst can reduce the risk of catalyst poisoning through the Cu foil reaction with dissolved sulfur that increases the CuSx catalyst average size and surface density for formate production. Another way to reduce the electrode poisoning by CO is by using metals that have low binding energy towards CO, such as Pd metal [124-126].

As shown in Table 1, the maximum operating time for formic acid production is 500 h in flow cell configuration using Sn/MWCNTs electrode [48]. The cell voltage remained almost constant throughout the 500 h, while a slight drop in the formic acid concentration (from 20 wt% to 15 wt%) occurred after 120 h. Whereas, the maximum operating time for formate is 152 h using $SnO_2$/ γ-$Al_2O_3$ supported on carbon fiber paper in H-type cell [127]. Considering the research papers demonstrated in Table 1, it seems that the type of support affects the electrode stability, which is by the nearly constant value of FE and current density. For instance, the FE reduced from 80% to 20% after 150 h of operation using $SnO_2$ supported on carbon fiber paper. However, for $SnO_2$ supported with γ-$A_2O_3$ and carbon fiber paper, the FE initially increased to 80% in 20 h, then slightly reduced to 70% after 150 h of operation [127]. Furthermore, the catholyte type affects the cell performance over long-term operation. For instance, the cumulative formate FE remained constant at 5% roughly during 30 min of operation in sodium carbonate electrolyte. On the other hand, the formate FE reduced from 80% to 15% during the same period in sodium bicarbonate [47].

The type of the electrolyte affects the cell stability. Wu et al.[55], reported that the $Na_2SO_4$ exhibited the most stable current density over 1 h compared to $K_2SO_4$ and $Cs_2SO_4$ at 0.5 M. after replacing the $SO_4^{2-}$ with $HCO_3^-$ of the same concentration, all electrolytes exhibited stable current density over the same period. In addition, the formate FE for Sn foil was investigated over 48 h in 0.5 M $KHCO_3$ and 0.5 M $Na_2SO_4$. The results revealed the formate FE decreased significantly by more than 50% for both electrolyte with obvious degradation during the first 10 h

**Fig. 11.** Pre-pilot plant unit for formate production [201].

of operation. Also, the deposition of trace metal presented as metal impurities, especially Zn, which is responsible for the reduction in FE. Furthermore, the electrolysis phase either liquid catholyte or catholyte free, influence the cell stability. Catholyte-free $CO_2$ ECR cells attain more stable current density and formate/formic acid FE. This is because the liquid catholyte in $CO_2$ ECR cells tends to damage the electrode as a result of the catholyte flow velocity and the excessive HER, which causes a reduction in formate/formic acid FE. For instance, Lee et al.[128], reported a stable formate FE at 91.2% for 48 h using Sn electrode, while the formate FE in liquid catholyte reduced from 67.7% to 31.8% during the same period.

During $CO_2$ ECR, the electrode goes through several structural changes as a result of long-term operation, which affects the overall cell performance. In fact, the morphology and the structure of the CL play an important role in defining the cell stability [129,130]. The deformation of the CL such as changes in the structural characteristics and pore size causes the cell performance in term of FE and current density to diminish in a short time (e.g. 10 h). For instance, the pore structure of Sn and Cu electrode totally collapse after 10 h of operation leaving a rod-branch overlapped structure. An alternative way to maintain the structural integrity and maintain a stable cell performance is by using alloyed electrodes. For example, $Cu_{6.2}Sn_5$ electrode maintained the structure integrity with little reduction in the pore diameter. Thereby, the electrode maintained a stable FE and current density value [35]. High catalyst stability can be achieved through optimizing the catalyst composition to maintain the structural integrity during the $CO_2$ ECR. Operational parameters such as electrolyte type and concentration should be investigated to optimize the cell performance and maintain its stability.

## 3.2. Operational parameters

### 3.2.1. $CO_2$ flow rate

In flow cells, the $CO_2$ flow rate affects the formate/formic acid FE and current density despite the cell configuration. For instance, in microfluidic cell, where the anodic and cathodic compartments are not separated by a membrane, as the $CO_2$ flow rate increases the current density increases significantly, but the $CO_2$ conversion efficiency decreases dramatically. This is because at higher flow rates the concentration boundary layer thickness decreases resulting in the need to apply higher current densities. Moreover, the reactant utilization decreases due to low residence time causing lower $CO_2$ conversion. Similar results were obtained in flow H-type cell, where the two compartments are separated by a membrane, and $CO_2$ gas and the electrolyte are flowing continuously. Furthermore, the influence of $CO_2$ flow rate on the formate FE is not significant at a current density below 300 mA/cm$^2$. However, at a current density above 300 mA/cm$^2$ the effect of $CO_2$ flow rate on formate FE becomes significant. Generally, as the $CO_2$ flow rate increases the formate FE increases up to a certain limit [42,50,179]. Beyond the optimum $CO_2$ flow rate, no enhancement in the formate FE could be detected. This is mainly because the $CO_2$ transportation to the active site is limited by the $CO_2$ mass transfer rate of the gas diffusion layer (macroscopic and microscopic layer). It is worth noting that the $CO_2$ mass transfer rate can be improved by optimizing the pore size and the thickness of the gas diffusion layer. Higher pore size and small thickness of the gas diffusion layer may increase the cell performance. Yet, higher pore size could increase the contact losses as the electrons travel through the solid matrix of the GDE, which could adversely affect the ECR cell performance [85,180].

It is worth mentioning that the flow rate of $CO_2$ and the electrolytes should be appropriately matched or else the electrolyte in the anodic chamber will run to the cathodic chamber and reduces the cell performance [181].

### 3.2.2. $CO_2$ feed pattern

Generally, the $CO_2$ is fed to the ECR cell either in a form of gaseous $CO_2$ or by saturating the electrolyte with $CO_2$ prior to starting the reduction process. In both cases, $CO_2$ should be 99.99% purity.

Therefore, varying the inlet $CO_2$ concentration does not have an effect on the performance of the ECR cell, yet it is claimed that the way that $CO_2$ is introduced has an effect [182]. Saturating the electrolyte with $CO_2$ results in the presence of bicarbonate and hydrogen ions. As mentioned, several research papers proved that bicarbonates electrolyte systems show poor formate FE and current density based on the assumption that the bicarbonates act as a substrate for the reduction process. On the other hand, $CO_2$ gas-fed system showed an enhanced performance. Therefore, it was suggested that $CO_2$ gas-fed system are more effective compared to $CO_2$ saturated electrolyte system [183]. Nevertheless, recently it has been proven that the $CO_2$ feed pattern does not influence the cell performance. In fact, bicarbonates act as carbon donors and supply $CO_2$ to the electrode surface, which is the substrate for the reduction process. Even in pure bicarbonates solution, $CO_2$ is the substrate for the reduction reaction [62,63,184]. Deng et al.[62] stated that the bicarbonate ions are not adsorbed on the catalyst layer, but are converted to $CO_2$ via equilibrium conversion which is adsorbed by the catalyst layer and reduced.

The local $CO_2$ concentration near the electrode is a critical factor that determines the ECR cell performance. Higher local $CO_2$ concentration at electrode/electrolyte interface leads to higher kinetics resulting in a better cell performance. The local $CO_2$ concentration is determined by several factors including catalyst's material, wettability, and pore structure, type of electrolyte, the electrolyte flow rate in flowing systems, and catalyst layer thickness [95,126]. In fact, the local environment of the CL and its properties controls the distribution of $CO_2$ influencing the cell performance. Uneven distribution of $CO_2$ can lead to poor catalyst utilization leading to poor cell performance [95]. Simulation results suggest that the thickness of the catalyst layer is the main factor that controls the $CO_2$ local concentration than the catalyst porosity [185]. Generally, higher local $CO_2$ concentration near the electrocatalyst leads to higher $CO_2$ reduction efficiency. The local $CO_2$ concentration can be increased by using a nanostructure needle shape electrocatalyst that is able to produce high local electric field that concentrates the electrolyte cations near the surface, which attracts the $HCO_3^-$ anions that are converted to $CO_2$ and thereby increases the $CO_2$ concentration [62].

### 3.2.3. Temperature

The majority of the studies on ECR of $CO_2$ into formate/formic acid are conducted at room temperature and atmospheric pressure, while the studies at elevated temperatures are scarce. Generally, as the operating temperature increases, the $CO_2$ diffusivity (mass transport) and kinetics increase. However, the $CO_2$ solubility decreases at a higher temperature, which decreases the local $CO_2$ concentration at the electrode/electrolyte interface resulting in a poor cell performance. This indicates that the local concentration of $CO_2$ at the electrode/electrolyte interface depends significantly on the $CO_2$ solubility. Despite that, several studies highlighted that increasing the temperature results in a higher current density and energy efficiency. Nevertheless, the HER rate increases with respect to $CO_2$ reduction rate due to low $CO_2$ solubility resulting in a low formate FE. It is reported that the optimum temperature required to suppress the HER rate and maximize the formate/formic acid FE falls between 0 ℃ and 35 ℃ [43], while others suggested an optimum temperature between 20 ℃ and 70 ℃ [186]. A study investigated the effect of temperature on the formic acid FE using Sn GDE electrode in H-type cell [83]. The results revealed as the temperature increases from 5 ℃ to 20 ℃, the formic acid FE increases from 0% to 60% followed by a considerable reduction in formic acid FE as the temperature elevates. In contrast, another study reported an optimum temperature of 50 ℃ showing an average formate FE of 85% for 24 h using $SnO_2$ GDE electrode in H-type cell [43]. Despite the fact that the system attains the lowest and most stable cathode potential at a temperature of 70 ℃,the cell performance was poor due to the increase in HER activity over formate production rate and the electrolyte residence time in the CL pores. It is worth mentioning that an increase in the electrolyte residence time causes electrode wetting that changes the catalyst structure and increases the electrodeposition on the metal impurities (e.g. Fe) from the electrolyte that boosts the HER activity. Therefore, temperature has strong correlation with the electrode wetting and degradation. Thus, it is important to operate the ECR cell at the optimum temperature to avoid the electrode degradation. For instance, Löwe et al.[43] highlighted that between 20 ℃ and 70 ℃, mechanical degradation was observed after 20 h of operation in form of small black fragments split off the GDE, but not at 50 ℃ which is the optimum temperature. This might be explained by the excessive HER that waken the GDE structure. It is worth noting that the catalyst type affects the optimum temperature that produces the maximum formic acid FE. For instance, lead, tin, and lead electrodes produces the highest formic acid FE at optimum temperature of 20 ℃, 20 ℃ and 60 ℃, respectively [187].

The effect of temperature on the formate FE varies in gas-phase (humidified $CO_2$ supply without using liquid catholyte) or liquid-phase (presence of liquid catholyte) ECR cell. As discussed above in liquid-phase ECR cell, as temperature increases beyond the optimum temperature the formate FE decreases. This reduction could be more than 30% for 20 ℃ temperature increment. However, in gas-phase ECR cell, the reduction in formate FE could be less than 10% for 20 ℃ temperature increment. This is ascribed to the fact that the $CO_2$ reduction reaction is not limited by the $CO_2$ solubility [128].

### 3.2.4. Pressure

$CO_2$ pressure has a significant effect on the product selectivity, FE, current density, electrolyte pH and formate/formic acid concentration. It is well-established in the literature that increasing the pressure increases the $CO_2$ solubility in the electrolyte (based on Henry's law) and facilitates working at high temperatures [188,189]. Most of the studies carried out the ECR under atmospheric pressure (≈1 bar(and few use high-pressure systems that requires pressurized stainless-steel cell in which the pressure can go up to 80 bars. In addition, some cell configurations are pressure sensitive such as membrane flow cell, which limits their operation under high pressure. The cell configurations described in this review can operate under high pressure by using stainless steel materials. It is worth noting that the cell configuration affects the $CO_2$ ECR efficiency under the same operating conditions. For instance, pressurized filter press cell showed formic acid concentration generated in 4 h 28% higher than the concentration generated by a pressurized cylindrical cell in 6 h under the same $CO_2$ pressure of 15 bars [190].

Furthermore, one of the greatest challenges in high-pressure ECR cells is the use of membrane with a good mechanical strength and low products cross over capability. As discussed, BPM membranes outperform AEM and CEM membrane and therefore it is used in pressurized systems. For instance, CEM membrane causes 4% formate cross-over, whereas BPM causes only 1% under the same pressure of 40 bars [86]. However, still the system suffers from formate/formic acid cross-over and must be eliminated to optimize the cell performance.

The $CO_2$ pressure has a significant influence on the $CO_2$ ECR cell performance. As the $CO_2$ pressure increases the formate/formic acid FE, current density, and concentration increase despite the electrode type. This is mainly because higher pressure results in higher $CO_2$ solubility enhancing the mass transfer to the CL [190,191]. For instance, a study reported that as the $CO_2$ pressure increases from 10 bars to 50 bars, the formic acid FE and concentration increases from 40% to 80%, and from 1500 ppm to 5000 ppm, respectively [86]. However, higher pressure would flatten out the formic acid FE and concentration and cause formic acid cross over through the BPM membrane. The analysis showed that at 50 bars, around 4% of formic acid was presented in the anodic compartment. In another study, the formate cross-over reached 1% under similar conditions [86]. The degree of crossover of formate and formic acid differs. Usually, formic acid has higher cross over intensity with respect to formate through the BPM [191].

Higher $CO_2$ pressure tend to reduce the electrolyte pH, but the amount of the reduction depends on the initial molarity of the electrolyte. For instance, as the $CO_2$ pressure increase from 1 bars to 70 bars, the pH reduces from 8.5 to 7 for 3 M $KHCO_3$, from 8.5 to 6.35 for 1 M $KHCO_3$, and from 8.5 to 5.35 for 0.1 M $KHCO_3$ as shown in Fig. 10a. However, for all electrolyte concentration, the pH does not reduce to a value below 5. The reduction of pH would favor the HER and determine the product distribution between formate and formic acid. As can be seen from Fig. 10b, between pH 6–7 the formate predominates. Thus, increasing the $CO_2$ pressure for all electrolyte concentration between 0.5 M and 3 M favors the formate production. On the other hand, increasing the $CO_2$ pressure for the low electrolyte concentration of 0.1 M still favors the formate production, but in lower quantities. If the formic acid is desired over formate, then pH below 3 showed be targeted, but that would adversely affect the electrode causing electrode depletion on the long-term operation and increases the HER activity [82,192].

The effect of $CO_2$ pressure on the formate/formic acid FE, current density and concentration differ for different electrolyte concentration and type. It is recommended to use intermediate electrolyte concentration such as 0.5 M $KHCO_3$ and 0.25 M $K_2SO_4$. This is because lower concentration could cause poor conductivity and significant pH drop, which enhance the HER and reduce the cell performance towards formate/formic acid production. Whereas higher concentration could cause the $CO_2$ solubility to decrease due to the salting-out effect, increase cation concentration on the electrode, and reduce the electrical field that destabilizes the intermediates [86].

Generally, it is stated in literature that increasing the $CO_2$ pressure might reduce the cathode overpotential. A study investigated the effect of $CO_2$ pressure on the formate/formic acid FE, current density, and concentration at different cell potentials [86]. First, for all cell potential, the formate/formic acid FE, current density and concentration increases as the $CO_2$ pressure elevate. Secondly, the results revealed that it is a challenge to obtain a high formate/formic acid FE, and current density at low cell potential, yet there is always a trade-off. For instance, at a low cell potential of 3 V, it is possible to obtain the highest formate/formic acid FE compared to cell potential of 4 V. In fact, the difference in FE remains above 30% under all $CO_2$ pressure that varies between 1 and 50 bars. On the other hand, the highest formate/formic acid current density can be obtained at cell potential of 4 V and the lowest at 3 V. That difference is more than 25 $mA/cm^2$ under all $CO_2$ pressure.

### 3.2.5. *Applied voltage*

In order to initiate the $CO_2$ ECR process, the voltage or current should be specified. The applied voltage affects the cell product distribution. As the applied voltage varies, products including hydrogen, carbon monoxide, methane, ethylene, formate, formic acid, methanol, ethanol, formaldehyde, isopropyl alcohol and other hydrocarbons and alcohol are produced. This occurs through multielectron transfer steps on an electrocatalyst. At low overpotential, formate and hydrogen are produced. As the overpotential increases the formate FE increases reaching the optimum value, while the Hydrogen FE decreases. However, as the overpotential increases further, the formate FE decreases, and hydrogen evolution dominates. Similarly, as the applied current changes, the product distribution changes. Therefore, the applied potential or current should be managed accordingly to optimize the cell performance towards formate/formic acid production [45,193].

Thus, the operational parameters have a critical role in the $CO_2$ ECR cell performance, stability, and sustainability. In addition, the effect of each operational parameter varies from one cell configuration to another. For instance, the $CO_2$ flow rate plays a critical role in defining the cell performance if the electrolyte is not saturated prior to its introduction. If the electrolyte is not saturated prior to its introduction to the cell, low $CO_2$ flow rate might result in poor cell performance due to insufficient $CO_2$ reactants. Similarly, high $CO_2$ flow rate might lead to poor cell performance due to low $CO_2$ residence time. In case the electrolyte is saturated with $CO_2$ prior to reduction process, the $CO_2$ flow rate does not have an effect on the cell performance. Eventhough high temperatures tend to increase the reaction kinetics, it reduces the $CO_2$ solubility in the electrolyte, which reduces the cell performance. Different types of working electrodes attain different optimum operating temperature, but the optimum temperature usually ranges from 20 ℃ to 70 ℃. On the other hand, increasing the pressure can effectively increases the $CO_2$ solubility, thereby increases the $CO_2$ conversion efficiency. However, a membrane with good mechanical strength should be used to prevent the products crossover. In addition, higher pressures can reduce the electrolyte pH, which might disturb and/or effect the conversion process. In order to overcome such a limitation, the use of high electrolyte concentration can facilitate operation at high pressure without a significant reduction in the electrolyte pH.

## 4. Large scale production

The implementation of $CO_2$ ECR on industrial scale is still at an early stage due to several challenges. The main obstacles that hinder the industrial application of $CO_2$ electrochemical conversion are: (1) high $CO_2$ separation and purification cost as $CO_2$ ECR requires 99.99% $CO_2$ (2), high energy consumption (3) the limited market is limited and less appealing to investors. Furthermore, there are several technological challenges associated with $CO_2$ ECR, including low catalyst activity, low product selectivity, poor catalyst stability, and non-optimized cell architecture for practical application [194,195]. In fact, the scale up of $CO_2$ ECR cell is a challenge as numerous factors and parameters must be considered and carefully managed to keep a stable cell performance. For industrial application, the cell should demonstrate a stable performance for at least 8000 h. In addition, it should demonstrate an overpotential below 1 V, current density between 200 and 1000 $mA/cm^2$ and formate/formic acid FE above 90% [123]. Another study mentioned that the cell should be stable for at least 20,000 h to be economically attractive [196]. Also, the cell membrane and electrode structure contribute to cell stability. Among all membranes reported, bipolar membrane is adequate for large scale application owing to its ability to maintain pH gradient, reduce the liquid crossover and promotes water dissociation at the interface [11,197]. Operating parameters, such as electrolyte type, flow rate, pH, and type of $CO_2$ feed can be optimized to maximize the cell performance. Currently, there are few number of large-scale $CO_2$ electrolyzers towards methane, CO, hydrocarbons and formic acid production [198,199]. Few research centers implemented the large-scale production of formate/formic acid through $CO_2$ ECR. For instance, In 2008, pilot plant was developed with a capacity of 146 kg $CO_2$/day resulting in around 110 kg formic acid/day at pressure around 10 bars [200]. Another recent scale up study reported the pre-pilot plant capacity of 55 kg $CO_2$/day that produces around 12 kg formate/day at atmospheric pressure (Fig. 11) [201].

Although the above-mentioned studies showed the applicability of this technology for scale-up production, several challenges need to be overcome to optimize the plant performance. One of the most important challenges is keeping a constant and relatively high current density (recommended $> 200$ $mA/cm^2$) over time. High value of current density indicates the reaction rate is high, which results in high formate/formic acid production rate. The current density is a strong function of the electrode (both support material and catalyst) properties and structure. Another challenge is the low energy efficiency. In a lab scale three compartments cell, the system showed energy efficiency of between 28% and 33% at current densities $>100$ $mA/cm^2$ over 1000 hr of operation [202]. While on pilot scale the energy efficiency is above 50% over 450 min of operation [200]. However, there is a lack of data regarding the energy efficiency of formic acid production on large/pilot scale. In order to keep a high cell energy efficiency, the FE should be high while the overpotential should be low. These parameters are mainly a strong function of the working electrode supporting material and catalyst properties as well as the anodic material. Furthermore, the membrane type is important since it can significantly reduce the IR drop between the cathodic and anodic compartments, thus reducing the cell overpotential resulting in a better energy efficiency. For industrial scale implementation, the FE is recommended to be above 90% and the potential between 2.5 and 3 V [203-205].

The cell design for $CO_2$ ECR to formate/formic acid for industrial implementation is still under development. In fact, each design has its own advantages and disadvantages. Yet, it seems that PEM cell configuration is a suitable design for scale-up. The PEM design showed relatively high FE towards formic acid production and stable cell operation over 500 h. However, several issues limit the PEM application in industry for $CO_2$ ECR to formate/formic acid as mentioned in Table 1 such as deterioration of membrane performance over time and GDE flooding. In fact, the mechanical strength of the membrane will definitely be a major issue when operating the cell at high pressure causing the formic acid cross over and membrane damage. Furthermore, more studies need to be conducted to improve the cell performance and stability. Eventhought the PEM cell showed FE of 94% and a stable performance for 500 h, the industrial scale requires cell operation for at least 8000 h with FE above 90%. Both cell design and operational parameters should be considered in order to develop a cell structure that can maintain a sustainable performance, meet the industrial operation requirements and be economically feasible. Nonetheless, membranes are expensive and require frequent replacement. From our point of view, more attention showed be given to membranelees $CO_2$ ECR cells to avoid frequent maintenance or membrane damage. In addition, the flooding of GDE with electrolyte that might damage the electrode structure and reduce the $CO_2$ conversion is another major issue. Gas-phase $CO_2$ ECR cells might prevent such problems, and thereby more research should be directed to those types of cells to develop efficient, stable, and sustainable $CO_2$ ECR cell.

## 5. Summary and future perspective

The electrochemical reduction of $CO_2$ is a promising technology that can effectively achieve a carbon–neutral economy through $CO_2$ electrochemical conversion to value-added chemicals, such as formate/formic acid. In this review, the mechanism of $CO_2$ electrochemical reduction to formate/formic acid and the electrolytic cell configuration used for formate/formic acid production were discussed. Also, the influence of the electrolytic cell design and operational parameters on the formate/formic acid FE, current density, and concentration were examined.

The cell design factors, such as cell architecture and membrane type have an important role in formate/formic acid production efficiency. In terms of cell configuration, H-type cell is suitable for testing the catalyst performance towards $CO_2$ electrochemical conversion to formate/formic acid, but not suitable for continuous operation and industrial application. One of the main drawbacks of H-type cell is the mass transport limitation due to low $CO_2$ solubility in electrolytes, and its unreliability for scale up and commercial use. However, flow cell and filter press cell show good mass transport, can be operated in continuous mode, and are easy to scale up. It is worth mentioning that the cell architecture affects the formate/formic acid production, such as channel length in the microfluidic cell. In addition, other design factors including electrolyte, membrane, and anode material should be considered to optimize the cell performance. The electrolyte can significantly enhance or render the cell performance. It is well-established in the literature that $KHCO_3$ outperforms other electrolytes. It is also recommended to use BPM over CEM and AEM, as it shows the lowest formate/formic acid crossover despite its short lifetime. Furthermore, anode plays an important role in the ECR cell. The selection of proper anode material can increase the cell efficiency, enhance formate/formic acid production and reduces the cell voltage. Also, the working electrode have a major role in $CO_2$ ECR process efficiency. To date, GDE outperforms other electrodes as it can effectively enhance mass transport, suppress HER using a proper support layer, and operates at high current density. Factors such as type of support layer, the thickness of support layer, catalyst type and catalyst properties should be optimized to enhance the cell performance. It is worth noting that the cell design parameters play a critical role in the cell configuration stability and performance. The operation with the suitable cell components (anode, membrane, electrolyte type and conditions and working electrode) can effectively boost the cell $CO_2$ ECR efficiency. For instance, PEM cell can be easily scaled up without a reduction in FE, yet it requires the use of proper electrolyte and membrane to maintain such performance. Also, the cell configuration is an important aspect of $CO_2$ ECR process to study and develop for effective application of $CO_2$ ECR on industrial scale. For example, controlling the cell configuration can determine the type of the product (formate or formic acid) as demonstrated in PEM cell discussion. Another example is that some cell configurations can prevent the cell flooding and/or dry-out such as microfluidic flow cell and allow zero gap arrangement and thus increasing the conversion efficiency, such as PEM cell. Operational parameters such as temperature, pressure, and $CO_2$ feed pattern should be carefully monitored to optimize the cell performance. All factors should be optimized to increase the local $CO_2$ concentration near the electrode to provide sufficient $CO_2$ (reactant) for the reduction reaction. Among all discussed operation factors, it seems that pressure, and electrolyte operational parameters (flow rate and pH) have a major role in defining the cell performance.

The literature shows a lack of studies related to developing affordable anodic material that can maintain a good cell performance. In addition, attention should be given to developing support layers that can suppress the HER and maintain good structural integrity of the GDE. Also, innovative cheap catalysts for selective $CO_2$ conversion to formate/formic acid with high production rate still need to be developed. Importantly, the catalyst should be feasible for industrial application. In addition, new cell architecture that can stabilize and provide smooth operation should be adopted for $CO_2$ conversion to formate/formic acid. Also, optimization of the cell design parameters such as channel length, catalyst layer thickness and anode material are needed. Moreover, experiments should be conducted on a pilot scale to assess the feasibility of the $CO_2$ electrochemical conversion to formate/formic acid. To date, studies on large scale $CO_2$ ECR process are scarce and most of them are on lab scale. The available research results hold significant promise for the applicability of $CO_2$ ECR on a commercial scale.

## Declaration of Competing Interest

The authors declare that they have no known competing financial interests or personal relationships that could have appeared to influence the work reported in this paper.

## Data availability

Data will be made available on request.

## Acknowledgment

The authors would like to acknowledge the support of Qatar National Research Fund (a member of Qatar Foundation) through Grant # NPRP 12 C-33923-SP-102 (NPRP12 C-0821-190017). The findings achieved herein are solely the responsibility of the authors. Open Access funding provided by the Qatar National Library.

## References

[1] Y.-Q. Geng, Y.-X. Guo, B. Fan, F.-Q. Cheng, H.-G. Cheng, Research progress of calcium-based adsorbents for $CO_2$ capture and anti-sintering modification, J. Fuel Chem. Technol. 49 (2021) 998–1013.

[2] J. Gong, N.J. English, D. Pant, G.R. Patzke, S. Protti, T. Zhang, Power-to-X: Lighting the Path to a Net-Zero-Emission Future, ACS Sustain. Chem. Eng. 9 (2021) 7179–7181.

[3] Y. Xiong, B. Wei, M. Wu, B. Hu, F. Zhu, J. Hao, W. Shi, Rapid synthesis of amorphous bimetallic copper-bismuth electrocatalysts for efficient

electrochemical $CO_2$ reduction to formate in a wide potential window, J. $CO_2$ Utiliz. 51 (2021), 101621.

[4] J. Zeng, K. Bejtka, W. Ju, M. Castellino, A. Chiodoni, A. Sacco, M. A. Farkhondehfal, S. Hernández, D. Rentsch, C. Battaglia, C.F. Pirri, Advanced Cu-Sn foam for selectively converting $CO_2$ to CO in aqueous solution, Appl. Catal. B 236 (2018) 475–482.

[5] X. Han, Q. Wang, Y. Wu, C. Wu, Boosting formate production from $CO_2$ electroreduction over gas diffusion electrode with accessible carbon mesopores, Electrochim. Acta 402 (2022), 139526.

[6] N.J. Claassens, C.A.R. Cotton, D. Kopljar, A. Bar-Even, Making quantitative sense of electromicrobial production, Nat. Catal. 2 (2019) 437–447.

[7] K. Van Daele, B. De Mot, M. Pupo, N. Daems, D. Pant, R. Kortlever, T. Breugelmans, Sn-based electrocatalyst stability: a crucial piece to the puzzle for the electrochemical $CO_2$ reduction toward formic acid, ACS Energy Lett. 6 (2021) 4317–4327.

[8] M.A. Green, Y. Hishikawa, E.D. Dunlop, D.H. Levi, J. Hohl-Ebinger, A.W.Y. Ho-Baillie, Solar cell efficiency tables (version 51), Prog. Photovolt. Res. Appl. 26 (2018) 3–12.

[9] L. Capital, Lazard's Levelized Cost of Energy Analysis-Version 7.0, in, 2013.

[10] X. Zhang, S.-X. Guo, K.A. Gandionco, A.M. Bond, J. Zhang, Electrocatalytic carbon dioxide reduction: from fundamental principles to catalyst design, Mater. Today Adv. 7 (2020), 100074.

[11] S.A. Al-Tamreh, M.H. Ibrahim, M.H. El-Naas, J. Vaes, D. Pant, A. Benamor, A. Amhamed, Electroreduction of Carbon Dioxide into Formate: A Comprehensive Review, ChemElectroChem 8 (2021) 3207–3220.

[12] S. Liang, N. Altaf, L. Huang, Y. Gao, Q. Wang, Electrolytic cell design for electrochemical $CO_2$ reduction, J. $CO_2$ Utiliz. 35 (2020) 90–105.

[13] P. Duarah, D. Haldar, V.S.K. Yadav, M.K. Purkait, Progress in the electrochemical reduction of $CO_2$ to formic acid: A review on current trends and future prospects, J. Environ. Chem. Eng. 9 (2021), 106394.

[14] R.I. Masel, Z. Liu, H. Yang, J.J. Kaczur, D. Carrillo, S. Ren, D. Salvatore, C. P. Berlinguette, An industrial perspective on catalysts for low-temperature $CO_2$ electrolysis, Nat. Nanotechnol. 16 (2021) 118–128.

[15] X. Zhang, X. Jiao, Y. Mao, X. Zhu, H. Kang, Z. Song, X. Yan, X. Yan, C. Han, L. Cui, K. Zhang, J. Qiao, A BiPb bimetallic electrode for highly selective $CO_2$ conversion to formate, Sep. Purif. Technol. 300 (2022), 121848.

[16] S. Guo, Y. Li, L. Liu, X. Zhang, S.J.a.C.P. Zhang, Theoretical evidence for new adsorption sites of $CO_2$ on the Ag electrode surface, (2020).

[17] H.N. Nong, L.J. Falling, A. Bergmann, M. Klingenhof, H.P. Tran, C. Spöri, R. Mom, J. Timoshenko, G. Zichittella, A. Knop-Gericke, S. Piccinin, J. Pérez-Ramírez, B. R. Cuenya, R. Schlögl, P. Strasser, D. Teschner, T.E. Jones, Key role of chemistry versus bias in electrocatalytic oxygen evolution, Nature 587 (2020) 408–413.

[18] B.A. Rosen, A. Salehi-Khojin, M.R. Thorson, W. Zhu, D.T. Whipple, P.J.A. Kenis, R.I. Masel, Ionic Liquid, 2013;Mediated Selective Conversion of $CO_2$ to CO at Low Overpotentials, 334 (2011) 643-644.

[19] Y. He, Q. He, L. Wang, C. Zhu, P. Golani, A.D. Handoko, X. Yu, C. Gao, M. Ding, X. Wang, F. Liu, Q. Zeng, P. Yu, S. Guo, B.I. Yakobson, L. Wang, Z.W. Seh, Z. Zhang, M. Wu, Q.J. Wang, H. Zhang, Z. Liu, Self-gating in semiconductor electrocatalysis, Nat. Mater. 18 (2019) 1098–1104.

[20] S. Popovic, M. Bele, N. Hodnik, Reconstruction of Copper Nanoparticles at Electrochemical $CO_2$ Reduction Reaction Conditions Occurs via Two-step Dissolution/Redeposition Mechanism, 8 (2021) 2634-2639.

[21] W. Schmickler, Electrochemical Theory: Double Layer, in: Reference Module in Chemistry, Molecular Sciences and Chemical Engineering, Elsevier, 2014.

[22] M. Khademi, D.P.J. Barz, Structure of the Electrical Double Layer Revisited: Electrode Capacitance in Aqueous Solutions, Langmuir 36 (2020) 4250–4260.

[23] K. Gandhi, Modeling of Effect of Double-Layer Capacitance and Failure of Lead-Acid Batteries in HRPSoC Application, J. Electrochem. Soc., 164 (2017) E3092-E3101.

[24] T. Tsuchiya, M. Takayanagi, K. Mitsuishi, M. Imura, S. Ueda, Y. Koide, T. Higuchi, K. Terabe, The electric double layer effect and its strong suppression at Li+ solid electrolyte/hydrogenated diamond interfaces, Commun. Chem. 4 (2021) 117.

[25] S. Liu, C. Wang, J. Wu, B. Tian, Y. Sun, Y. Lv, Z. Mu, Y. Sun, X. Li, F. Wang, Y. Wang, L. Tang, P. Wang, Y. Li, M. Ding, Efficient $CO_2$ Electroreduction with a Monolayer $Bi_2WO_6$ through a Metallic Intermediate Surface State, ACS Catal. 11 (2021) 12476–12484.

[26] Y. Ito, S. Kukunuri, S. Jeong, G. Elumalai, A.A. Haji Tajuddin, Z. Xi, K. Hu, T. Ohto, Phase-dependent electrochemical $CO_2$ reduction ability of NiSn alloys for formate generation, ACS Appl. Energy Mater. 4 (2021) 7122–7128.

[27] Y. Chen, M.W. Kanan, Tin oxide dependence of the $CO_2$ Reduction efficiency on tin electrodes and enhanced activity for tin/tin oxide thin-film catalysts, J. Am. Chem. Soc. 134 (2012) 1986–1989.

[28] A.A. Peterson, J.K. Nørskov, Activity descriptors for $CO_2$ electroreduction to methane on transition-metal catalysts, J. Phys. Chem. Lett. 3 (2012) 251–258.

[29] R. Kortlever, J. Shen, K.J.P. Schouten, F. Calle-Vallejo, M.T.M. Koper, Catalysts and reaction pathways for the electrochemical reduction of carbon dioxide, J. Phys. Chem. Lett. 6 (2015) 4073–4082.

[30] J.S. Yoo, R. Christensen, T. Vegge, J.K. Nørskov, F. Studt, Theoretical Insight into the Trends that Guide the Electrochemical Reduction of Carbon Dioxide to Formic Acid, ChemSusChem 9 (2016) 358–363.

[31] M.F. Baruch, J.E. Pander, J.L. White, A.B. Bocarsly, Mechanistic Insights into the Reduction of $CO_2$ on Tin Electrodes using in Situ ATR-IR Spectroscopy, ACS Catal. 5 (2015) 3148–3156.

[32] Z. Sun, T. Ma, H. Tao, Q. Fan, B. Han, Fundamentals and Challenges of Electrochemical $CO_2$ Reduction Using Two-Dimensional Materials, Chem 3 (2017) 560–587.

[33] J.T. Feaster, C. Shi, E.R. Cave, T. Hatsukade, D.N. Abram, K.P. Kuhl, C. Hahn, J. K. Nørskov, T.F. Jaramillo, Understanding Selectivity for the Electrochemical Reduction of Carbon Dioxide to Formic Acid and Carbon Monoxide on Metal Electrodes, ACS Catal. 7 (2017) 4822–4827.

[34] S. Zhao, S. Li, T. Guo, S. Zhang, J. Wang, Y. Wu, Y. Chen, Advances in Sn-Based Catalysts for Electrochemical $CO_2$ Reduction, Nano-Micro Letters 11 (2019) 62.

[35] S. Ning, J. Wang, D. Xiang, S. Huang, W. Chen, S. Chen, X. Kang, Electrochemical reduction of $SnO_2$ to Sn from the Bottom: In-Situ formation of $SnO_2$/Sn heterostructure for highly efficient electrochemical reduction of carbon dioxide to formate, J. Catal. 399 (2021) 67–74.

[36] Q. Xie, G.O. Larrazábal, M. Ma, I. Chorkendorff, B. Seger, J. Luo, Copper-indium hydroxides derived electrocatalysts with tunable compositions for electrochemical $CO_2$ reduction, J. Energy Chem. 63 (2021) 278–284.

[37] X. Jiang, X. Wang, Z. Liu, Q. Wang, X. Xiao, H. Pan, M. Li, J. Wang, Y. Shao, Z. Peng, Y. Shen, M. Wang, A highly selective tin-copper bimetallic electrocatalyst for the electrochemical reduction of aqueous $CO_2$ to formate, Appl Catal B 259 (2019), 118040.

[38] Z. Yang, H. Wang, X. Fei, W. Wang, Y. Zhao, X. Wang, X. Tan, Q. Zhao, H. Wang, J. Zhu, L. Zhou, H. Ning, M. Wu, MOF derived bimetallic CuBi catalysts with ultra-wide potential window for high-efficient electrochemical reduction of $CO_2$ to formate, Appl Catal B 298 (2021), 120571.

[39] H. Jiang, Y. Zhao, L. Wang, Y. Kong, F. Li, P. Li, Electrochemical $CO_2$ reduction to formate on Tin cathode: Influence of anode materials, J. $CO_2$ Utiliz. 26 (2018) 408–414.

[40] T. Hatsukade, K.P. Kuhl, E.R. Cave, D.N. Abram, T.F. Jaramillo, Insights into the electrocatalytic reduction of $CO_2$ on metallic silver surfaces, PCCP 16 (2014) 13814–13819.

[41] L.-X. Liu, Y. Zhou, Y.-C. Chang, J.-R. Zhang, L.-P. Jiang, W. Zhu, Y. Lin, Tuning $Sn_3O_4$ for $CO_2$ reduction to formate with ultra-high current density, Nano Energy 77 (2020), 105296.

[42] Y. Qian, Y. Liu, H. Tang, B.-L. Lin, Highly efficient electroreduction of $CO_2$ to formate by nanorod@2D nanosheets SnO, J. $CO_2$ Utiliz. 42 (2020), 101287.

[43] A. Löwe, C. Rieg, T. Hierlemann, N. Salas, D. Kopljar, N. Wagner, E. Klemm, The Influence of Temperature on the Performance of Gas Diffusion Electrodes in $CO_2$ Reduction Reaction, ChemElectroChem 6 (2019).

[44] R. Kas, R. Kortlever, H. Yılmaz, M.T.M. Koper, G. Mul, Manipulating the Hydrocarbon Selectivity of Copper Nanoparticles in $CO_2$ Electroreduction by Process Conditions, ChemElectroChem 2 (2015) 354–358.

[45] K.P. Kuhl, E.R. Cave, D.N. Abram, T.F. Jaramillo, New insights into the electrochemical reduction of carbon dioxide on metallic copper surfaces, Energ. Environ. Sci. 5 (2012) 7050–7059.

[46] R.A. Tufa, D. Chanda, M. Ma, D. Aili, T.B. Demissie, J. Vaes, Q. Li, S. Liu, D. Pant, Towards highly efficient electrochemical $CO_2$ reduction: Cell designs, membranes and electrocatalysts, Appl. Energy 277 (2020), 115557.

[47] S. Narayan, B. Haines, J. Soler, T. Valdez, Electrochemical Conversion of Carbon Dioxide to Formate in Alkaline Polymer Electrolyte Membrane Cells, J. Electrochem. Soc., 158 (2011) A167-A173.

[48] H. Yang, J.J. Kaczur, S.D. Sajjad, R.I. Masel, Electrochemical conversion of $CO_2$ to formic acid utilizing SustainionTM membranes, J. CO2 Utiliz. 20 (2017) 208–217.

[49] D.T. Whipple, E.C. Finke, P.J.A. Kenis, Microfluidic Reactor for the Electrochemical Reduction of Carbon Dioxide: The Effect of pH, Electrochem. Solid St. 13 (2010) B109.

[50] H. Wang, D.Y.C. Leung, J. Xuan, Modeling of a microfluidic electrochemical cell for $CO_2$ utilization and fuel production, Appl. Energy 102 (2013) 1057–1062.

[51] M. Alvarez-Guerra, A. Del Castillo, A. Irabien, Continuous electrochemical reduction of carbon dioxide into formate using a tin cathode: Comparison with lead cathode, Chem. Eng. Res. Des. 92 (2014) 692–701.

[52] G. Díaz-Sainz, M. Alvarez-Guerra, J. Solla-Gullón, L. García-Cruz, V. Montiel, A. Irabien, $CO_2$ electroreduction to formate: Continuous single-pass operation in a filter-press reactor at high current densities using Bi gas diffusion electrodes, J. $CO_2$ Utiliz. 34 (2019) 12–19.

[53] A. Castillo, M. Alvarez-Guerra, A. Irabien, Continuous Electroreduction of $CO_2$ to Formate Using Sn Gas Diffusion Electrodes, AIChE J 60 (2014) 3557–3564.

[54] B. Liu, B.S. Mahmood, E. Mohammadian, A. Khaksar Manshad, N.R. Rosli, M. Ostadhassan, Measurement of Solubility of $CO_2$ in NaCl, $CaCl_2$, $MgCl_2$ and $MgCl_2$ + $CaCl_2$ Brines at Temperatures from 298 to 373 K and Pressures up to 20 MPa Using the Potentiometric Titration Method, 14 (2021) 7222.

[55] J. Wu, F.G. Risalvato, F.-S. Ke, P.J. Pellechia, X.-D. Zhou, Electrochemical Reduction of Carbon Dioxide I. Effects of the Electrolyte on the Selectivity and Activity with Sn Electrode, J. Electrochem. Soc., 159 (2012) F353-F359.

[56] K. Hara, A. Kudo, T. Sakata, M. Watanabe, High Efficiency Electrochemical Reduction of Carbon Dioxide under High Pressure on a Gas Diffusion Electrode Containing Pt Catalysts, J. Electrochem. Soc., 142 (1995) L57-L59.

[57] J. Wu, F. Risalvato, X.-D. Zhou, Effects of the Electrolyte on Electrochemical Reduction of $CO_2$ on Sn Electrode, ChemPhysChem 20 (2012).

[58] X. Han, Z. Yu, J. Qu, T. Qi, W. Guo, G. Zhang, Measurement and Correlation of Solubility Data for $CO_2$ in $NaHCO_3$ Aqueous Solution, J. Chem. Eng. Data 56 (2011) 1213–1219.

[59] C.S. Wong, P.Y. Tishchenko, W.K. Johnson, Solubility of Carbon Dioxide in Aqueous HCl and $NaHCO_3$ Solutions from 278 to 298 K, J. Chem. Eng. Data 50 (2005) 817–821.

[60] Y. Guan, X. Zhang, Y. Zhang, T.N.V. Karsili, M. Fan, Y. Liu, B. Marchetti, X.-D. Zhou, Achieving high selectivity towards electro-conversion of $CO_2$ using In-doped Bi derived from metal-organic frameworks, J. Colloid Interface Sci. 612 (2022) 235–245.

[61] X. Wang, Y. Zou, Y. Zhang, B. Marchetti, Y. Liu, J. Yi, X.-D. Zhou, J. Zhang, Tin-based metal organic framework catalysts for high-efficiency electrocatalytic $CO_2$ conversion into formate, J. Colloid Interface Sci. 626 (2022) 836–847.

[62] W. Deng, T. Yuan, S. Chen, H. Li, C. Hu, H. Dong, B. Wu, T. Wang, J. Li, G.A. Ozin, J. Gong, Effect of bicarbonate on $CO_2$ electroreduction over cathode catalysts, Fundamental Research 1 (2021) 432–438.

[63] A. Goyal, G. Marcandalli, V.A. Mints, M.T.M. Koper, Competition between $CO_2$ Reduction and Hydrogen Evolution on a Gold Electrode under Well-Defined Mass Transport Conditions, J. Am. Chem. Soc. 142 (2020) 4154–4161.

[64] R. Kortlever, K.H. Tan, Y. Kwon, M.T.M. Koper, Electrochemical carbon dioxide and bicarbonate reduction on copper in weakly alkaline media, J. Solid State Electrochem. 17 (2013) 1843–1849.

[65] O. Gutiérrez-Sánchez, N. Daems, W. Offermans, Y.Y. Birdja, M. Bulut, D. Pant, T. Breugelmans, The inhibition of the proton donor ability of bicarbonate promotes the electrochemical conversion of $CO_2$ in bicarbonate solutions, J. $CO_2$ Utiliz. 48 (2021), 101521.

[66] A. Wuttig, Y. Yoon, J. Ryu, Y. Surendranath, Bicarbonate Is Not a General Acid in Au-Catalyzed $CO_2$ Electroreduction, J. Am. Chem. Soc. 139 (2017) 17109–17113.

[67] J. Zhang, W. Luo, A. Züttel, Crossover of liquid products from electrochemical $CO_2$ reduction through gas diffusion electrode and anion exchange membrane, J. Catal. 385 (2020) 140–145.

[68] C.M. Gabardo, C.P. O'Brien, J.P. Edwards, C. McCallum, Y. Xu, C.-T. Dinh, J. Li, E.H. Sargent, D. Sinton, Continuous Carbon Dioxide Electroreduction to Concentrated Multi-carbon Products Using a Membrane Electrode Assembly, Joule 3 (2019) 2777–2791.

[69] K. Ito, T. Murata, S. Ikeda, Electrochemical reduction of carbon dioxide to organic compounds, Bull. Nagoya Inst. Tech. (1976) 209–214.

[70] Y.Z. Wei, P. Chiang, S. Sridhar, Ion size effects on the dynamic and static dielectric properties of aqueous alkali solutions, J. Chem. Phys. 96 (1992) 4569–4573.

[71] C. Guo, S. Chen, Y. Zhang, G. Wang, Solubility of $CO_2$ in Nonaqueous Absorption System of 2-(2-Aminoethylamine)ethanol + Benzyl Alcohol, J. Chem. Eng. Data 59 (2014) 1796–1801.

[72] H. Coskun, A. Aljabour, P. De Luna, D. Farka, T. Greunz, D. Stifter, M. Kus, X. Zheng, M. Liu, W. Hassel Achim, W. Schöfberger, H. Sargent Edward, S. Sariciftci Niyazi, P. Stadler, Biofunctionalized conductive polymers enable efficient $CO_2$ electroreduction, Sci. Adv. 3 (2017).

[73] M. König, S.-H. Lin, J. Vaes, D. Pant, E. Klemm, Integration of aprotic $CO_2$ reduction to oxalate at a Pb catalyst into a GDE flow cell configuration, Faraday Discuss. 230 (2021) 360–374.

[74] C.M. Gabardo, A. Seifitokaldani, J.P. Edwards, C.-T. Dinh, T. Burdyny, M. G. Kibria, C.P. O'Brien, E.H. Sargent, D. Sinton, Combined high alkalinity and pressurization enable efficient $CO_2$ electroreduction to CO, Energ. Environ. Sci. 11 (2018) 2531–2539.

[75] T.C. Berto, L. Zhang, R.J. Hamers, J.F. Berry, Electrolyte Dependence of $CO_2$ Electroreduction: Tetraalkylammonium Ions Are Not Electrocatalysts, ACS Catal. 5 (2015) 703–707.

[76] H. Coskun, A. Aljabour, P. De Luna, D. Farka, T. Greunz, D. Stifter, M. Kus, X. Zheng, M. Liu, A.W.J.S.A. Hassel, Biofunctionalized conductive polymers enable efficient CO2 electroreduction, 3 (2017).

[77] C. Amatore, J.M. Saveant, Mechanism and kinetic characteristics of the electrochemical reduction of carbon dioxide in media of low proton availability, J. Am. Chem. Soc. 103 (1981) 5021–5023.

[78] A. Shamsuri, D. Abdullah, Ionic liquids: Preparations and limitations, MAKARA, SAINS 14 (2010) 101–106.

[79] V. Küpers, J.F. Dohmann, P. Bieker, M. Winter, T. Placke, M. Kolek, Opportunities and Limitations of Ionic Liquid- and Organic Carbonate Solvent-Based Electrolytes for Mg-Ion-Based Dual-Ion Batteries, ChemSusChem 14 (2021) 4480–4498.

[80] D. Kopljar, A. Inan, P. Vindayer, N. Wagner, E. Klemm, Electrochemical reduction of $CO_2$ to formate at high current density using gas diffusion electrodes, J. Appl. Electrochem. 44 (2014) 1107–1116.

[81] W. Lv, R. Zhang, P. Gao, L. Lei, Studies on the faradaic efficiency for electrochemical reduction of carbon dioxide to formate on tin electrode, J. Power Sources 253 (2014) 276–281.

[82] A.R.T. Morrison, V. van Beusekom, M. Ramdin, L.J.P. van den Broeke, T.J. H. Vlugt, W. de Jong, Modeling the Electrochemical Conversion of Carbon Dioxide to Formic Acid or Formate at Elevated Pressures, J. Electrochem. Soc. 166 (2019) E77–E86.

[83] H.-Y. Kim, I. Choi, S.H. Ahn, S.J. Hwang, S.J. Yoo, J. Han, J. Kim, H. Park, J. H. Jang, S.-K. Kim, Analysis on the effect of operating conditions on electrochemical conversion of carbon dioxide to formic acid, Int. J. Hydrogen Energy 39 (2014) 16506–16512.

[84] O. Scialdone, A. Galia, G.L. Nero, F. Proietto, S. Sabatino, B. Schiavo, Electrochemical reduction of carbon dioxide to formic acid at a tin cathode in divided and undivided cells: effect of carbon dioxide pressure and other operating parameters, Electrochim. Acta 199 (2016) 332–341.

[85] X. Lu, D.Y.C. Leung, H. Wang, J. Xuan, A high performance dual electrolyte microfluidic reactor for the utilization of $CO_2$, Appl. Energy 194 (2017) 549–559.

[86] M. Ramdin, A.R.T. Morrison, M. de Groen, R. van Haperen, R. de Kler, L.J.P. van den Broeke, J.P.M. Trusler, W. de Jong, T.J.H. Vlugt, High Pressure Electrochemical Reduction of $CO_2$ to Formic Acid/Formate: A Comparison between Bipolar Membranes and Cation Exchange Membranes, Ind. Eng. Chem. Res. 58 (2019) 1834–1847.

[87] K. Subramanian, K. Asokan, D. Jeevarathinam, M. Chandrasekaran, Electrochemical membrane reactor for the reduction of carbondioxide to formate, J. Appl. Electrochem. 37 (2007) 255–260.

[88] S.S. Hosseiny, M. Wessling, 13 - Ion exchange membranes for vanadium redox flow batteries, in: A. Basile, S.P. Nunes (Eds.) Advanced Membrane Science and Technology for Sustainable Energy and Environmental Applications, Woodhead Publishing, 2011, pp. 413-434.

[89] H. Strathmann, A. Grabowski, G. Eigenberger, Ion-Exchange Membranes in the Chemical Process Industry, Ind. Eng. Chem. Res. 52 (2013) 10364–10379.

[90] M. Wang, B. Xu, Q. Zou, X. Dong, R. Shao, J. Qiao, Graphene oxide prompted double-crosslinked Poly(vinyl alcohol)/Poly(diallyldimethylammonium chloride) Anion-exchange membrane for superior $CO_2$ electrochemical reduction, Sep. Purif. Technol. 307 (2023), 122792.

[91] R.S. Reiter, W. White, S. Ardo, Communication—Electrochemical Characterization of Commercial Bipolar Membranes under Electrolyte Conditions Relevant to Solar Fuels Technologies, J. Electrochem. Soc., 163 (2015) H3132-H3134.

[92] Q. Zou, X. Guo, L. Gao, F. Hong, J. Qiao, Fabrication of bacterial cellulose membrane-based alkaline-exchange membrane for application in electrochemical reduction of $CO_2$, Sep. Purif. Technol. 272 (2021), 118910.

[93] L. Peng, Y. Wang, Y. Wang, N. Xu, W. Lou, P. Liu, D. Cai, H. Huang, J. Qiao, Separated growth of Bi-Cu bimetallic electrocatalysts on defective copper foam for highly converting $CO_2$ to formate with alkaline anion-exchange membrane beyond $KHCO_3$ electrolyte, Appl Catal B 288 (2021), 120003.

[94] J. He, Y. Li, A. Huang, Q. Liu, C. Li, Electrolyzer and Catalysts Design from Carbon Dioxide to Carbon Monoxide Electrochemical Reduction, Electrochem. Energy Rev. 4 (2021) 680–717.

[95] L.-C. Weng, A.T. Bell, A.Z. Weber, Modeling gas-diffusion electrodes for $CO_2$ reduction, PCCP 20 (2018) 16973–16984.

[96] G. Díaz-Sainz, M. Alvarez-Guerra, A. Irabien, Continuous electrochemical reduction of $CO_2$ to formate: comparative study of the influence of the electrode configuration with Sn and Bi-based electrocatalysts, Molecules 25 (2020).

[97] S. Perathoner, M. Gangeri, P. Lanzafame, G. Centi, Nanostructured electrocatalytic Pt-carbon materials for fuel cells and $CO_2$ conversion, Kinet. Catal. 48 (2007) 877–883.

[98] S.C. Perry, P.-K. Leung, L. Wang, C. Ponce de León, Developments on carbon dioxide reduction: Their promise, achievements, and challenges, Curr. Opin. Electrochem. 20 (2020) 88–98.

[99] Q. Wang, H. Dong, H. Yu, H. Yu, Enhanced performance of gas diffusion electrode for electrochemical reduction of carbon dioxide to formate by adding polytetrafluoroethylene into catalyst layer, J. Power Sources 279 (2015) 1–5.

[100] J. Wu, F.G. Risalvato, S. Ma, X.-D. Zhou, Electrochemical reduction of carbon dioxide III. The role of oxide layer thickness on the performance of Sn electrode in a full electrochemical cell, J. Mater. Chem. A 2 (2014) 1647–1651.

[101] Y.-H. Cho, H.-S. Park, Y.-H. Cho, I.-S. Park, Y.-E. Sung, The improved methanol tolerance using Pt/C in cathode of direct methanol fuel cell, Electrochim. Acta 53 (2008) 5909–5912.

[102] C.S. Kim, Y.G. Chun, D.H. Peck, D.R. Shin, A novel process to fabricate membrane electrode assemblies for proton exchange membrane fuel cells, Int. J. Hydrogen Energy 23 (1998) 1045–1048.

[103] D. Bevers, N. Wagner, M. Von Bradke, Innovative production procedure for low cost PEFC electrodes and electrode/membrane structures, Int. J. Hydrogen Energy 23 (1998) 57–63.

[104] S. Nur Ubaidah, K.K. Ying, N.I. Khuan, Electrodeposition: Principles, Applications and Methods, in: NTC 2011: Nuclear Technical Convention 2011, Malaysia, 2011.

[105] H. Rabiee, L. Ge, X. Zhang, S. Hu, M. Li, Z. Yuan, Gas diffusion electrodes (GDEs) for electrochemical reduction of carbon dioxide, carbon monoxide, and dinitrogen to value-added products: a review, Energ. Environ. Sci. 14 (2021) 1959–2008.

[106] H. Wang, J. Jia, P. Song, Q. Wang, D. Li, S. Min, C. Qian, L. Wang, Y.F. Li, C. Ma, T. Wu, J. Yuan, M. Antonietti, G.A. Ozin, Efficient Electrocatalytic Reduction of $CO_2$ by Nitrogen-Doped Nanoporous Carbon/Carbon Nanotube Membranes: A Step Towards the Electrochemical $CO_2$ Refinery, Angew. Chem. Int. Ed. 56 (2017) 7847–7852.

[107] J. Wu, P.P. Sharma, B.H. Harris, X.-D. Zhou, Electrochemical reduction of carbon dioxide: IV dependence of the Faradaic efficiency and current density on the microstructure and thickness of tin electrode, J. Power Sources 258 (2014) 189–194.

[108] A.A. Kulikovsky, Analytical model of the anode side of DMFC: the effect of non-Tafel kinetics on cell performance, Electrochem. Commun. 5 (2003) 530–538.

[109] Z. Chen, N. Wang, S. Yao, L. Liu, The flaky Cd film on Cu plate substrate: An active and efficient electrode for electrochemical reduction of $CO_2$ to formate, J. $CO_2$ Utiliz. 22 (2017) 191–196.

[110] S. Zhang, P. Kang, T.J. Meyer, Nanostructured Tin Catalysts for Selective Electrochemical Reduction of Carbon Dioxide to Formate, J. Am. Chem. Soc. 136 (2014) 1734–1737.

[111] F. Li, L. Chen, G.P. Knowles, D.R. MacFarlane, J. Zhang, Hierarchical Mesoporous $SnO_2$ Nanosheets on Carbon Cloth: A Robust and Flexible Electrocatalyst for $CO_2$ Reduction with High Efficiency and Selectivity, Angew. Chem. Int. Ed. 56 (2017) 505–509.

[112] B. Xu, I. Masood Ul Hasan, L. Peng, J. Liu, N. Xu, M. Fan, N.K. Niazi, J. Qiao, Anion-regulation engineering toward Cu/In/MOF bimetallic electrocatalysts for selective electrochemical reduction of $CO_2$ to CO/formate, Materials Reports: Energy, 2 (2022) 100139.

[113] Q. Wang, C. Zhu, C. Wu, H. Yu, Direct synthesis of bismuth nanosheets on a gas diffusion layer as a high-performance cathode for a coupled electrochemical

system capable of electroreduction of $CO_2$ to formate with simultaneous degradation of organic pollutants, Electrochim. Acta 319 (2019) 138–147.
[114] R. Zhang, W. Lv, L. Lei, Role of the oxide layer on Sn electrode in electrochemical reduction of $CO_2$ to formate, Appl. Surf. Sci. 356 (2015) 24–29.
[115] M. Bevilacqua, J. Filippi, A. Lavacchi, A. Marchionni, H.A. Miller, W. Oberhauser, E. Vesselli, F. Vizza, Energy Savings in the Conversion of $CO_2$ to Fuels using an Electrolytic Device, Energ. Technol. 2 (2014) 522–525.
[116] G. Tao, K.R. Sridhar, C.L. Chan, Study of carbon dioxide electrolysis at electrode/electrolyte interface: Part II. Pt-YSZ cermet/YSZ interface, Solid State Ionics 175 (2004) 621–624.
[117] R. Zhang, W. Lv, G. Li, M.A. Mezaal, L. Lei, Electrochemical reduction of carbon dioxide to formate with a Sn cathode and an $IrxSnyRuzO_2$/Ti anode, RSC Adv. 5 (2015) 68662–68667.
[118] S. Ma, R. Luo, S. Moniri, Y. Lan, P.J.A. Kenis, Efficient Electrochemical Flow System with Improved Anode for the Conversion of $CO_2$ to CO, J. Electrochem. Soc., 161 (2014) F1124-F1131.
[119] N. Han, P. Ding, L. He, Y. Li, Y. Li, Promises of Main Group Metal-Based Nanostructured Materials for Electrochemical $CO_2$ Reduction to Formate, Adv. Energy Mater. 10 (2020) 1902338.
[120] R. Zhang, W. Lv, G. Li, M.A. Mezaal, X. Li, L. Lei, Retarding of electrochemical oxidation of formate on the platinum anode by a coat of Nafion membrane, J. Power Sources 272 (2014) 303–310.
[121] M. Dunwell, Q. Lu, J. Heyes, J. Rosen, J. Chen, Y. Yan, F. Jiao, B. Xu, The Central Role of Bicarbonate in the Electrochemical Re- duction of Carbon Dioxide on Gold, J. Am. Chem. Soc. 139 (2017).
[122] A. Wuttig, M. Yaguchi, K. Motobayashi, M. Osawa, Y. Surendranath, Inhibited proton transfer enhances Au-catalyzed $CO_2$-to-fuels selectivity, Proc. Natl. Acad. Sci. 113 (2016) 201602984.
[123] S. Verma, B. Kim, H.-R.-M. Jhong, S. Ma, P.J.A. Kenis, A Gross-Margin Model for Defining Technoeconomic Benchmarks in the Electroreduction of $CO_2$, ChemSusChem 9 (2016) 1972–1979.
[124] A. Klinkova, P. De Luna, C.-T. Dinh, O. Voznyy, E.M. Larin, E. Kumacheva, E. H. Sargent, Rational Design of Efficient Palladium Catalysts for Electroreduction of Carbon Dioxide to Formate, ACS Catal. 6 (2016) 8115–8120.
[125] J.W. Lim, W.J. Dong, J.Y. Park, D.M. Hong, J.-L. Lee, Spontaneously Formed CuSx Catalysts for Selective and Stable Electrochemical Reduction of Industrial $CO_2$ Gas to Formate, ACS Appl. Mater. Interfaces 12 (2020) 22891–22900.
[126] S. Jin, Z. Hao, K. Zhang, Z. Yan, J. Chen, Advances and Challenges for the Electrochemical Reduction of $CO_2$ to CO: From Fundamentals to Industrialization, Angew. Chem. Int. Ed. 60 (2021) 20627–20648.
[127] Y.E. Kim, W. Lee, M.H. Youn, S.K. Jeong, H.J. Kim, J.C. Park, K.T. Park, Leaching-resistant $SnO_2$/γ-$Al_2O_3$ nanocatalyst for stable electrochemical $CO_2$ reduction into formate, J. Ind. Eng. Chem. 78 (2019) 73–78.
[128] W. Lee, Y.E. Kim, M.H. Youn, S.K. Jeong, K.T. Park, Catholyte-Free Electrocatalytic $CO_2$ Reduction to Formate, Angew. Chem. Int. Ed. 57 (2018) 6883–6887.
[129] H. Ge, Z. Gu, P. Han, H. Shen, A.M. Al-Enizi, L. Zhang, G. Zheng, Mesoporous tin oxide for electrocatalytic $CO_2$ reduction, J. Colloid Interface Sci. 531 (2018) 564–569.
[130] H. Zhong, Y. Qiu, T. Zhang, X. Li, H. Zhang, X. Chen, Bismuth nanodendrites as a high performance electrocatalyst for selective conversion of $CO_2$ to formate, J. Mater. Chem. A 4 (2016) 13746–13753.
[131] H. Zhong, Y. Qiu, X. Li, L. Pan, H. Zhang, Ordered cone-structured tin directly grown on carbon paper as efficient electrocatalyst for $CO_2$ electrochemical reduction to formate, J. Energy Chem. 55 (2021) 236–243.
[132] Q. Xie, G.O. Larrazábal, M. Ma, I. Chorkendorff, B. Seger, J. Luo, Copper-indium hydroxides derived electrocatalysts with tunable compositions for electrochemical $CO_2$ reduction, J. Energy Chem. (2021).
[133] Z. Qin, X. Jiang, Y. Cao, S. Dong, F. Wang, L. Feng, Y. Chen, Y. Guo, Nitrogen-doped porous carbon derived from digested sludge for electrochemical reduction of carbon dioxide to formate, Sci. Total Environ. 759 (2021), 143575.
[134] H. Jiang, L. Wang, Y. Li, B. Gao, Y. Guo, C. Yan, M. Zhuo, H. Wang, S. Zhao, High-selectivity electrochemical $CO_2$ reduction to formate at low overpotential over Bi catalyst with hexagonal sheet structure, Appl. Surf. Sci. 541 (2021), 148577.
[135] H. Zheng, G. Wu, G. Gao, X. Wang, The bismuth architecture assembled by nanotubes used as highly efficient electrocatalyst for $CO_2$ reduction to formate, Chem. Eng. J. 421 (2021), 129606.
[136] J. Wang, S. Ning, M. Luo, D. Xiang, W. Chen, X. Kang, Z. Jiang, S. Chen, In-Sn alloy core-shell nanoparticles: In-doped SnOx shell enables high stability and activity towards selective formate production from electrochemical reduction of $CO_2$, Appl Catal B 288 (2021), 119979.
[137] F. Zhang, C. Chen, S. Yan, J. Zhong, B. Zhang, Z. Cheng, Cu@Bi nanocone induced efficient reduction of $CO_2$ to formate with high current density, Appl. Catal. A 598 (2020), 117545.
[138] F. Li, Efficient electrochemical reduction of $CO_2$ to formate using Sn-Polyaniline film on Ni foam, Electrochim. Acta 332 (2020), 135457.
[139] B. Bohlen, D. Wastl, J. Radomski, V. Sieber, L. Vieira, Electrochemical $CO_2$ reduction to formate on indium catalysts prepared by electrodeposition in deep eutectic solvents, Electrochem. Commun. 110 (2020), 106597.
[140] Q. Hu, M. Xu, S. Hu, P.-L. Tremblay, T. Zhang, Selective electrocatalytic reduction of carbon dioxide to formate by a trimetallic Sn-Co/Cu foam electrode, J. Electroanal. Chem. 877 (2020), 114623.
[141] B. Zha, C. Li, J. Li, Efficient electrochemical reduction of $CO_2$ into formate and acetate in polyoxometalate catholyte with indium catalyst, J. Catal. 382 (2020) 69–76.
[142] D. Wu, W. Chen, X. Wang, X.-Z. Fu, J.-L. Luo, Metal-support interaction enhanced electrochemical reduction of $CO_2$ to formate between graphene and Bi nanoparticles, J. $CO_2$ Utiliz. 37 (2020) 353–359.
[143] L. Li, F. Cai, F. Qi, D.-K. Ma, Cu nanowire bridged Bi nanosheet arrays for efficient electrochemical $CO_2$ reduction toward formate, J. Alloy. Compd. 841 (2020), 155789.
[144] M.J.W. Blom, V. Smulders, W.P.M. van Swaaij, S.R.A. Kersten, G. Mul, Pulsed electrochemical synthesis of formate using Pb electrodes, Appl Catal B 268 (2020), 118420.
[145] M. Zhao, Y. Gu, W. Gao, P. Cui, H. Tang, X. Wei, H. Zhu, G. Li, S. Yan, X. Zhang, Z. Zou, Atom vacancies induced electron-rich surface of ultrathin Bi nanosheet for efficient electrochemical $CO_2$ reduction, Appl Catal B 266 (2020), 118625.
[146] D. Zhang, Z. Tao, F. Feng, B. He, W. Zhou, J. Sun, J. Xu, Q. Wang, L. Zhao, High efficiency and selectivity from synergy: Bi nanoparticles embedded in nitrogen doped porous carbon for electrochemical reduction of $CO_2$ to formate, Electrochim. Acta 334 (2020), 135563.
[147] D. Li, L. Huang, T. Liu, J. Liu, L. Zhen, J. Wu, Y. Feng, Electrochemical reduction of carbon dioxide to formate via nano-prism assembled CuO microspheres, Chemosphere 237 (2019), 124527.
[148] Y. Xing, M. Cui, P. Fan, J. Ren, C. Zhang, N. Li, X. Wen, X. Ji, Efficient and selective electrochemical reduction of $CO_2$ to formate on 3D porous structured multi-walled carbon nanotubes supported Pb nanoparticles, Mater. Chem. Phys. 237 (2019), 121826.
[149] X. Wang, W. Xiao, J. Zhang, Z. Wang, X. Jin, Nanoporous Ag-Sn derived from codeposited AgCl-$SnO_2$ for the electrocatalytic reduction of $CO_2$ with high formate selectivity, Electrochem. Commun. 102 (2019) 52–56.
[150] Q. Zhang, J. Du, A. He, Z. Liu, C. Tao, Low overpotential electrochemical $CO_2$ reduction to formate on $Co_3O_4$–$CeO_2$/low graphitic carbon catalyst with oxygen vacancies, J. Solid State Chem. 279 (2019), 120946.
[151] S. Rasul, A. Pugnant, H. Xiang, J.-M. Fontmorin, E.H. Yu, Low cost and efficient alloy electrocatalysts for $CO_2$ reduction to formate, J. $CO_2$ Utiliz. 32 (2019) 1–10.
[152] J. Huang, X. Guo, Y. Wei, Q. Hu, X. Yu, L. Wang, A renewable, flexible and robust single layer nitrogen-doped graphene coating Sn foil for boosting formate production from electrocatalytic $CO_2$ reduction, J. $CO_2$ Utiliz. 33 (2019) 166–170.
[153] K. Mou, Z. Chen, S. Yao, L. Liu, Enhanced electrochemical reduction of carbon dioxide to formate with in-situ grown indium-based catalysts in an aqueous electrolyte, Electrochim. Acta 289 (2018) 65–71.
[154] S. Liu, F. Pang, Q. Zhang, R. Guo, Z. Wang, Y. Wang, W. Zhang, J. Ou, Stable nanoporous Sn/$SnO_2$ composites for efficient electroreduction of $CO_2$ to formate over wide potential range, Appl. Mater. Today 13 (2018) 135–143.
[155] Q. Shi, J. Wu, S. Mu, Direct experimental evidence and low reduction potentials for the electrochemical reduction of $CO_2$ on fluorine doped tin oxide semiconductor, J. Electroanal. Chem. 820 (2018) 1–8.
[156] A. Aljabour, H. Coskun, D.H. Apaydin, F. Ozel, A.W. Hassel, P. Stadler, N. S. Sariciftci, M. Kus, Nanofibrous cobalt oxide for electrocatalysis of $CO_2$ reduction to carbon monoxide and formate in an acetonitrile-water electrolyte solution, Appl Catal B 229 (2018) 163–170.
[157] H.-P. Yang, Q. Lin, H.-W. Zhang, Y. Wu, L.-D. Fan, X.-Y. Chai, Q.-L. Zhang, J.-H. Liu, C.-X. He, Selective electrochemical reduction of $CO_2$ by a binder-free platinum/nitrogen-doped carbon nanofiber/copper foil catalyst with remarkable efficiency and reusability, Electrochem. Commun. 93 (2018) 138–142.
[158] M. Fan, C. Ma, T. Lei, J. Jung, D. Guay, J. Qiao, Aqueous-phase electrochemical reduction of $CO_2$ based on $SnO_2CuO$ nanocomposites with improved catalytic activity and selectivity, Catal. Today 318 (2018) 2–9.
[159] Y. Qiu, J. Du, W. Dong, C. Dai, C. Tao, Selective conversion of $CO_2$ to formate on a size tunable nano-Bi electrocatalyst, J. $CO_2$ Utiliz. 20 (2017) 328–335.
[160] S. Kim, W.J. Dong, S. Gim, W. Sohn, J.Y. Park, C.J. Yoo, H.W. Jang, J.-L. Lee, Shape-controlled bismuth nanoflakes as highly selective catalysts for electrochemical carbon dioxide reduction to formate, Nano Energy 39 (2017) 44–52.
[161] W. Lv, J. Zhou, J. Bei, R. Zhang, L. Wang, Q. Xu, W. Wang, Electrodeposition of nano-sized bismuth on copper foil as electrocatalyst for reduction of $CO_2$ to formate, Appl. Surf. Sci. 393 (2017) 191–196.
[162] Q. Lai, N. Yang, G. Yuan, Highly efficient In–Sn alloy catalysts for electrochemical reduction of $CO_2$ to formate, Electrochem. Commun. 83 (2017) 24–27.
[163] J. Yu, H. Liu, S. Song, Y. Wang, P. Tsiakaras, Electrochemical reduction of carbon dioxide at nanostructured $SnO_2$/carbon aerogels: The effect of tin oxide content on the catalytic activity and formate selectivity, Appl. Catal. A 545 (2017) 159–166.
[164] T. Takashima, T. Suzuki, H. Irie, Electrochemical carbon dioxide reduction on copper-modified palladium nanoparticles synthesized by underpotential deposition, Electrochim. Acta 229 (2017) 415–421.
[165] X. Zhang, T. Lei, Y. Liu, J. Qiao, Enhancing $CO_2$ electrolysis to formate on facilely synthesized Bi catalysts at low overpotential, Appl Catal B 218 (2017) 46–50.
[166] A. Rabiee, D. Nematollahi, Electrochemical reduction of $CO_2$ to formate ion using nanocubic mesoporous In$(OH)_3$/carbon black system, Mater. Chem. Phys. 193 (2017) 109–116.
[167] Y. Fu, Y. Li, X. Zhang, Y. Liu, X. Zhou, J. Qiao, Electrochemical $CO_2$ reduction to formic acid on crystalline $SnO_2$ nanosphere catalyst with high selectivity and stability, Chin. J. Catal. 37 (2016) 1081–1088.
[168] Y. Fu, Y. Li, X. Zhang, Y. Liu, J. Qiao, J. Zhang, D.P. Wilkinson, Novel hierarchical $SnO_2$ microsphere catalyst coated on gas diffusion electrode for enhancing energy efficiency of $CO_2$ reduction to formate fuel, Appl. Energy 175 (2016) 536–544.
[169] C. Zhao, J. Wang, Electrochemical reduction of $CO_2$ to formate in aqueous solution using electro-deposited Sn catalysts, Chem. Eng. J. 293 (2016) 161–170.

[170] Y. Wang, J. Zhou, W. Lv, H. Fang, W. Wang, Electrochemical reduction of $CO_2$ to formate catalyzed by electroplated tin coating on copper foam, Appl. Surf. Sci. 362 (2016) 394–398.

[171] H. Xiang, H.A. Miller, M. Bellini, H. Christensen, K. Scott, S. Rasul, E.H. Yu, Production of formate by $CO_2$ electrochemical reduction and its application in energy storage, Sustainable, Energy Fuel 4 (2020) 277–284.

[172] R. Kortlever, I. Peters, S. Koper, M.T.M. Koper, Electrochemical $CO_2$ Reduction to Formic Acid at Low Overpotential and with High Faradaic Efficiency on Carbon-Supported Bimetallic Pd–Pt Nanoparticles, ACS Catal. 5 (2015) 3916–3923.

[173] X. Zhu, K. Gupta, M. Bersani, J.A. Darr, P.R. Shearing, D.J.L. Brett, Electrochemical reduction of carbon dioxide on copper-based nanocatalysts using the rotating ring-disc electrode, Electrochim. Acta 283 (2018) 1037–1044.

[174] H. Liu, B. Miao, H. Chuai, X. Chen, S. Zhang, X. Ma, Nanoporous tin oxides for efficient electrochemical $CO_2$ reduction to formate, Green, Chem. Eng. (2021).

[175] T. Lei, X. Zhang, J. Jung, Y. Cai, X. Hou, Q. Zhang, J. Qiao, Continuous electroreduction of carbon dioxide to formate on Tin nanoelectrode using alkaline membrane cell configuration in aqueous medium, Catal. Today 318 (2018) 32–38.

[176] E. Bertin, S. Garbarino, C. Roy, S. Kazemi, D. Guay, Selective electroreduction of $CO_2$ to formate on Bi and oxide-derived Bi films, J. $CO_2$ Utiliz. 19 (2017) 276–283.

[177] A. Del Castillo, M. Alvarez-Guerra, J. Solla-Gullón, A. Sáez, V. Montiel, A. Irabien, Sn nanoparticles on gas diffusion electrodes: Synthesis, characterization and use for continuous $CO_2$ electroreduction to formate, J. $CO_2$ Utiliz. 18 (2017) 222–228.

[178] A. Del Castillo, M. Alvarez-Guerra, J. Solla-Gullón, A. Sáez, V. Montiel, A. Irabien, Electrocatalytic reduction of $CO_2$ to formate using particulate Sn electrodes: Effect of metal loading and particle size, Appl. Energy 157 (2015) 165–173.

[179] K. Wu, E. Birgersson, P.J.A. Kenis, I.A. Karimi, Modeling and Simulating Electrochemical Reduction of $CO_2$ in a Microfluidic Cell, in: M.R. Eden, J.D. Siirola, G.P. Towler (Eds.) Computer Aided Chemical Engineering, Elsevier, 2014, pp. 639-644.

[180] T. Berning, N. Djilali, Three-dimensional computational analysis of transport phenomena in a PEM fuel cell—a parametric study, J. Power Sources 124 (2003) 440–452.

[181] Y.-H. Wang, W.-J. Jiang, W. Yao, Z.-L. Liu, Z. Liu, Y. Yang, L.-Z. Gao, Advances in electrochemical reduction of carbon dioxide to formate over bismuth-based catalysts, Rare Met. 40 (2021) 2327–2353.

[182] A. Bonet Navarro, A. Nogalska, R. Garcia-Valls, Direct Electrochemical Reduction of Bicarbonate to Formate Using Tin Catalyst, Electrochem, 2 (2021).

[183] N. Sreekanth, K.L. Phani, Selective reduction of $CO_2$ to formate through bicarbonate reduction on metal electrodes: new insights gained from SG/TC mode of SECM, Chem. Commun. 50 (2014) 11143–11146.

[184] O. Gutiérrez-Sánchez, B. de Mot, M. Bulut, D. Pant, T. Breugelmans, Engineering Aspects for the Design of a Bicarbonate Zero-Gap Flow Electrolyzer for the Conversion of $CO_2$ to Formate, ACS Appl. Mater. Interfaces (2022).

[185] T. Jaster, A. Gawel, D. Siegmund, J. Holzmann, H. Lohmann, E. Klemm, U.-P. Apfel, Electrochemical $CO_2$ reduction toward multicarbon alcohols - The microscopic world of catalysts & process conditions, iScience 25 (2022), 104010.

[186] A. Löwe, C. Rieg, T. Hierlemann, N. Salas, D. Kopljar, N. Wagner, E. Klemm, Influence of Temperature on the Performance of Gas Diffusion Electrodes in the $CO_2$ Reduction Reaction, ChemElectroChem 6 (2019) 4497–4506.

[187] T. Mizuno, K. Ohta, A. Sasaki, T. Akai, M. Hirano, A. Kawabe, Effect of Temperature on Electrochemical Reduction of High-Pressure $CO_2$ with In, Sn, and Pb Electrodes, Energy Source. 17 (1995) 503–508.

[188] B. Endrődi, G. Bencsik, F. Darvas, R. Jones, K. Rajeshwar, C. Janáky, Continuous-flow electroreduction of carbon dioxide, Prog. Energy Combust. Sci. 62 (2017) 133–154.

[189] D.U. Nielsen, X.-M. Hu, K. Daasbjerg, T. Skrydstrup, Chemically and electrochemically catalysed conversion of $CO_2$ to CO with follow-up utilization to value-added chemicals, Nature, Catalysis 1 (2018) 244–254.

[190] F. Proietto, B. Schiavo, A. Galia, O. Scialdone, Electrochemical conversion of $CO_2$ to HCOOH at tin cathode in a pressurized undivided filter-press cell, Electrochim. Acta 277 (2018) 30–40.

[191] F. Köleli, D. Balun, Reduction of $CO_2$ under high pressure and high temperature on Pb-granule electrodes in a fixed-bed reactor in aqueous medium, Appl. Catal. A 274 (2004) 237–242.

[192] X. Lu, D.Y.C. Leung, H. Wang, M.M. Maroto-Valer, J. Xuan, A pH-differential dual-electrolyte microfluidic electrochemical cells for $CO_2$ utilization, Renew. Energy 95 (2016) 277–285.

[193] Y. Deng, Y. Huang, D. Ren, A.D. Handoko, Z.W. Seh, P. Hirunsit, B.S. Yeo, On the Role of Sulfur for the Selective Electrochemical Reduction of $CO_2$ to Formate on CuSx Catalysts, ACS Appl. Mater. Interfaces 10 (2018) 28572–28581.

[194] J. Qiao, Y. Liu, F. Hong, J. Zhang, A review of catalysts for the electroreduction of carbon dioxide to produce low-carbon fuels, Chem. Soc. Rev. 43 (2014) 631–675.

[195] D. Du, R. Lan, J. Humphreys, S. Tao, Progress in inorganic cathode catalysts for electrochemical conversion of carbon dioxide into formate or formic acid, J. Appl. Electrochem. 47 (2017) 661–678.

[196] R. Lin, J. Guo, X. Li, P. Patel, A. Seifitokaldani, Electrochemical Reactors for $CO_2$ Conversion 10 (2020) 473.

[197] Y.C. Li, D. Zhou, Z. Yan, R.H. Gonçalves, D.A. Salvatore, C.P. Berlinguette, T. E. Mallouk, Electrolysis of $CO_2$ to Syngas in Bipolar Membrane-Based Electrochemical Cells, ACS Energy Lett. 1 (2016) 1149–1153.

[198] N. Sridhar, D. Hill, A. Agarwal, Y. Zhai, E.J.D.N.V. Hektor, G. Lloyd, Carbon Dioxide Utilization. Electrochemical Conversion of $CO_2$–Opportunities and Challenges, (2011).

[199] O.G. Sánchez, Y.Y. Birdja, M. Bulut, J. Vaes, T. Breugelmans, D. Pant, Recent advances in industrial $CO_2$ electroreduction, Current Opinion in Green and Sustainable, Chemistry 16 (2019) 47–56.

[200] C. Oloman, H. Li, Continuous Co-Current Electrochemical Reduction of Carbon Dioxide, in, Google Patents (2008).

[201] D.K. Akrivi Asimakopoulou, M. Mouratidis, G. Pantoleontos, T. Damartzis, Georgios Skevis Recycling carbon dioxide in the cement industry to produce added-value additives: a step towards a $CO_2$ circular economy, in, Recode Project (2019).

[202] H. Yang, J.J. Kaczur, S.D. Sajjad, R.I. Masel, Performance and long-term stability of $CO_2$ conversion to formic acid using a three-compartment electrolyzer design, J. $CO_2$ Utiliz. 42 (2020), 101349.

[203] M. Jouny, W. Luc, F. Jiao, General Techno-Economic Analysis of $CO_2$ Electrolysis Systems, Ind. Eng. Chem. Res. 57 (2018) 2165–2177.

[204] A.J. Martín, G.O. Larrazábal, J. Pérez-Ramírez, Towards sustainable fuels and chemicals through the electrochemical reduction of $CO_2$: lessons from water electrolysis, Green Chem. 17 (2015) 5114–5130.

[205] F. Proietto, U. Patel, A. Galia, O. Scialdone, Electrochemical conversion of $CO_2$ to formic acid using a Sn based electrode: A critical review on the state-of-the-art technologies and their potential, Electrochim. Acta 389 (2021), 138753.